

# POLITECNICO DI TORINO

CORSO DI LAUREA MAGISTRALE IN INGEGNERIA MECCANICA



TESI DI LAUREA MAGISTRALE

MODELLING AND DESIGN OF A FLEXIBLE CONNECTOR  
FOR MODULAR FLOATING PLATFORMS

**Relatori:** Giovanni Bracco  
Giuliana Mattiazzo  
Sergej Antonello Sirigu

**Candidato:** Vincenzo Boccanfuso

ANNO ACCADEMICO 2022/2023

## Summary

1. Introduction .....	4
2. State of the art .....	6
2.1 <i>Floating platforms</i> .....	6
2.2 <i>Connector systems</i> .....	8
3. Elastomeric bearings .....	12
3.1 <i>Elastomeric bearings: uses and features</i> .....	14
3.2 <i>Parametric modelling</i> .....	16
3.3 <i>Stiffness and geometrical parameters</i> .....	19
4. Dynamics of multibody system.....	25
4.1 <i>Connector stiffness matrix</i> .....	25
4.2 <i>Regular wave analysis</i> .....	34
4.3 <i>Irregular wave analysis</i> .....	43
4.4 <i>Comfort Criteria</i> .....	52
5. Connection design.....	55
5.1 <i>Constructive solution</i> .....	55
5.2 <i>Equivalent stiffness</i> .....	57
5.3 <i>Bearings Dimensioning</i> .....	59
Conclusions and future developments.....	67
Bibliography.....	69
Appendix .....	72



# 1. Introduction

Since 1961, global average sea level has risen at an average rate of 1.8 mm/year and accelerated to 3.1 mm/year in 1993, with contributions from thermal expansion [1]. Approximately 70% of the world's population live within 100 miles of seacoasts, and nearly 50 million people now live at risk of coastal flooding and displacement by tidal and storm surges. Sea levels are anticipated to rise by another 7.6–91.4 cm by 2025 due to a combination of polar icecap and glacial meltdown, increased precipitation, coastal land erosion and subsidence, and unpredictable thermal expansion from rising seawater temperatures [1]. Furthermore, to date, 2.4 billion people live in coastal communities (40% of the global population) and the demand for urban space is on the rise because of demographic and urbanization processes. A modular floating structure (MFS) which is composed of hexagonal floating modules provides a feasible way to create useable land on the sea to solve the challenges brought from the increasing population and land scarcity of coastal cities. Compared with the traditional very large floating structures (VLFS), the production, transportation, installation, and maintenance of the MFS are more convenient, more importantly, it can greatly reduce the hydroelastic response of the structure [2] [3]. Furthermore, VLFS are usually designed to serve a single purpose (e.g. airport, storage facility etc.) and are not considered a viable alternative for residential development. The hypothesis is that MFS offers a unique, new, and sustainable solution for addressing issues related to coastal urbanization and global sea level rise, for example these systems can be used to support the emerging floating renewables industry as a logistics support base, for O&M operations and the installation of processing plants. Further applications may include support for aquaculture, seaweed farming and vertical farming activities for countries suffering from land shortages; or the creation of floating port terminals to solve the problem of shipping congestion.

The MFS concept has the potential to solve all these deficiencies by using medium size (relative to operated ship sizes) rigid modules that create a large-scale consolidated platform for urban development. These floating modules or ‘Building Units’ can be designed ad-hoc for any urban purpose (e.g. residential, recreational facilities, parks, etc.), and can be arranged and rearranged in numerous spatial configurations. This facilitates future growth and development, as it can be realized by simply adding new modules in correlation to actual

demand. Typical offshore structures are too industrial and robust for “normative” urban applications, and perhaps even too expensive. Therefore, to bring the urban MFS concept into realization, there is a need to narrow the gap between currently available engineering solutions (technology) and architectural design (concept). The proposed MFS concept aims to narrow this gap by providing engineering solutions, and design methodologies, suitable for urban needs offshore.

It is practically not possible to construct just single rigid body floating structure for the purposes due to high stresses induced by the sea waves and high cost of transportation or manufacturing [4]. To tackle this, the platforms can be connected together to produce a large platform such a way that the high forces are damped by the connectors. The primary objective of this study is the design of a connection between the platforms, with particular interest in the correlation between connector parameters and hydroelastic responses of the MFS.

The problem of reducing the hydroelastic response has been analyzed by several researchers [2][3], and the most common solution is to increase structural stiffness at the expense of higher costs due to additional construction materials needed. Another attractive solution involves the use of semi-rigid connectors instead of rigid ones to relax the structural loads. The modular solution allows the individual platform to be considered as a rigid body simplifying the numerical modelling and reducing the computational time to simulate the system. This method is called “rigid module, flexible connector” (RMFC) approach [5], and it assumes that the modules are more rigid than the connections where deformations are concentrated, reducing the size of the numerical model. The proper design of connector stiffness can positively affect the hydroelastic response of modular floating islands (MFI) with reduction of structural loads, and thus it represents the most significant design parameter [6] [7]. Results of Jiang et Al. [8] showed that compared to the responses of rigid connectors, flexible hinge-type or semi-rigid connector can effectively reduce the hydroelastic responses of MFI system.

## 2. State of the art

### 2.1 Floating platforms

The realisation of floating communities is extremely strategic in the future perspective of rising seas due to climate change and, in the short term, to solve the problem of land shortage, nowadays suffered by a large number of territories. The idea of creating land for human activities from the sea is not new. The technique of land reclamation is well known and used for creating new land [4] from sea and consists of filling the area with inert material and building protective walls with devastating impacts on local environmental balances [9]. Another promising and environmentally less impactful solution is the creation of land on the sea through the so-called very large floating structures (VLFS). VLFS are artificial portions of land on the sea anchored to the seabed and can be divided into two major categories the semi-submersible type and pontoon-type.

The basic idea is to create “land on sea” by connecting a number of standardized modular units to form the desired size and shape for generic applications. Floating platforms are large structures that can float in the open sea which can be useful for different activities from storage facility to landing runway platforms.

The relative motion between adjacent floating structure consists of six components, grouped into translational motions (surge, sway, and heave) and rotational motions (pitch, roll and yaw), as shown in the Figure 2.1.

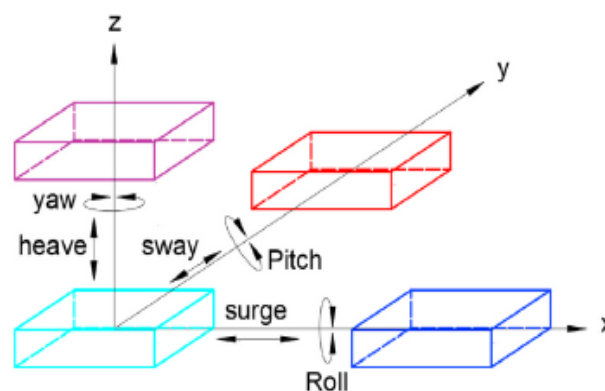


**Figure 2.1** translational motions and rotational motions

Among all the parameters to be evaluated, the main ones are module size, which determines the overall dimensions including, but not limited to draft and edge lengths, and module shape, referring to the curvature of the hull lines, this design category is of particular importance due to the modular approach. Most architectural renderings of modular floating platforms have presented solutions based on equilateral triangular, quadrangular, or hexagonal footprints. Each shape has advantages and disadvantages when considering e.g., transport and response to waves or on-board logistics and storage and the choice is not straightforward, since it affects the whole design.

The choice fell on the hexagonal platform, which allows a spatial arrangement as shown in the Figure 2.2:

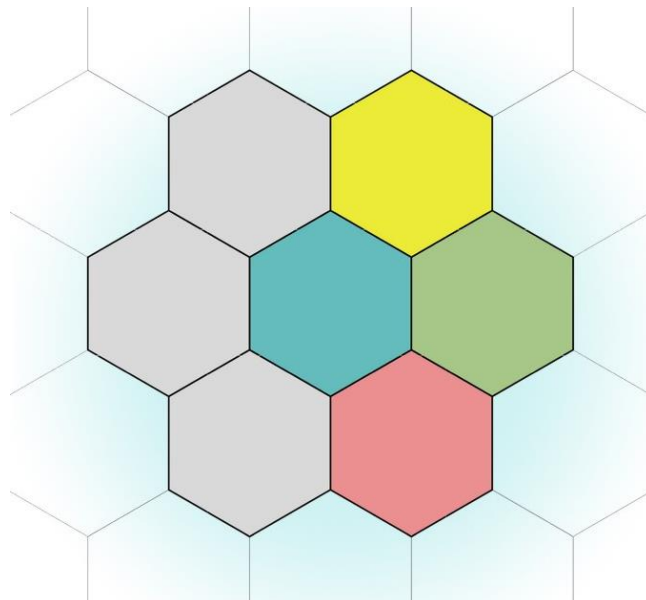


*Figure 2.2 hexagonal platform spatial arrangement*

To create a large structure that floats, it is only practical to joint small structures so to tackle the unwanted loads by the sea waves. These small structures can be connected by means of flexible connector which can act as a damper to the wave motion so to create a stable floating platform. Both rigid and flexible connectors have positive and negative aspects, summarized in Figure 2.3.

Type	Positive Aspects	Negative Aspects
Rigid Connector System	<ul style="list-style-type: none"> <li>• Small or no motions</li> <li>• Easy internal transport of containers</li> <li>• Complies with crane track requirements</li> </ul>	<ul style="list-style-type: none"> <li>• Large connection forces</li> <li>• Complex connection configuration</li> <li>• Difficult to decouple the connectors</li> </ul>
Flexible Connector System	<ul style="list-style-type: none"> <li>• Low connection forces</li> <li>• Easy decoupling process</li> </ul>	<ul style="list-style-type: none"> <li>• Large motion amplitude</li> <li>• Complex internal transport</li> <li>• Flexible platform deck</li> </ul>

*Figure 2.3 Connector systems*

Since the structure is floating in the sea, the consideration of hydro elastic responses is very important. The safety of these floating platforms depends on the hydro elastic response. The study of the flexible joints shows that the semi- rigid joints can reduce the hydro elastic response in a significant amount.

## *2.2 Connector systems*

The massive single continuum structure may suffer large bending stress and induce many problems in manufacturing as well as transportation. A single continuum structure may not a good design for VLFS, while the modularization seems a better choice. Large floating structures are occasionally made of several modules with space in between to improve mobility. In such cases, the rigidity of connector systems is designed in accordance with different practical situations, including rigid connector system, vertical-free connector system, hinge connector system and fully flexible connector system.

For multimodular floating systems, the connector between modules becomes the weakest component in the whole system, which is subjected to large loads and is easily damaged. These connectors are designed to avoid the failure due to high stresses that can arise in the connectors due to the dynamic behaviour of the sea. One of the technical challenges is to find the stiffness of the connecting system according to the practical situation.

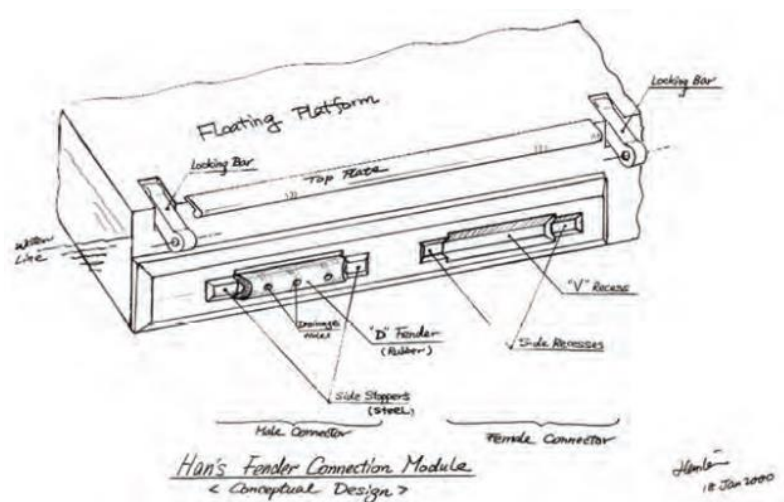
Apart from being acting as a simple connector between platforms, there is more functions that needed to be satisfied by these connectors. For example, the connector is also

responsible for the alignment of the platforms in the open sea, safety of the platforms by damping, reduction of construction or assembling time and so on.

Type & Direction of connector	Extra restrained DOF.		
	Allowed DOF by 1 connector	2 hinges, (hor.) next to each other	2 hinges, (vert.) above each other
Centre point short face	all rotations 	roll, yaw 	pitch 
Centre point long face	all rotations 	pitch, yaw 	roll 
Vertical element long face	Yaw 	Yaw 	- 
Horizontal element short face	Pitch 	Yaw 	pitch 
Horizontal element long face	Roll 	yaw 	roll 

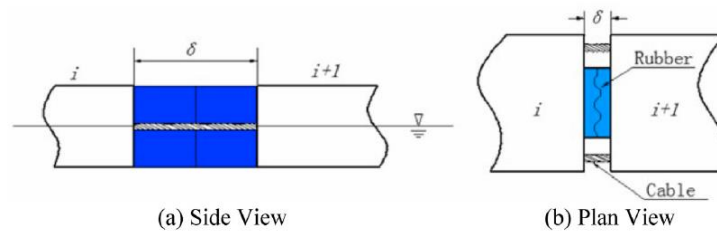
**Figure 2.4** Types and direction of connectors

Figure 2.5 shows a connection module where alternative male and female type connectors are used to join the platforms together. With this concept, the self-aligning capability as well as the secure connection with the damping effect can be achieved.



**Figure 2.5** connection module with alternative male and female type connectors

There are different methods and concepts to connect the large floating structure together in the open sea so that the connection can be stable with the response of the sea waves. Due to the large structure of floating platform, there will be high loads in the connections. A better idea is to provide a flexible joint to connect the adjacent floating platform with considerable amount of stiffness. There are various flexible connector concepts published which varies in their designs and material.



**Figure 2.6** example of flexible connection

In the article by Huai et al. [10], a type of structural design for a flexible connection for connecting the platforms is discussed. Here, there will be a male and a female part of the connector where the combination of steel and rubber material is used to produce the flexibility in the connector.

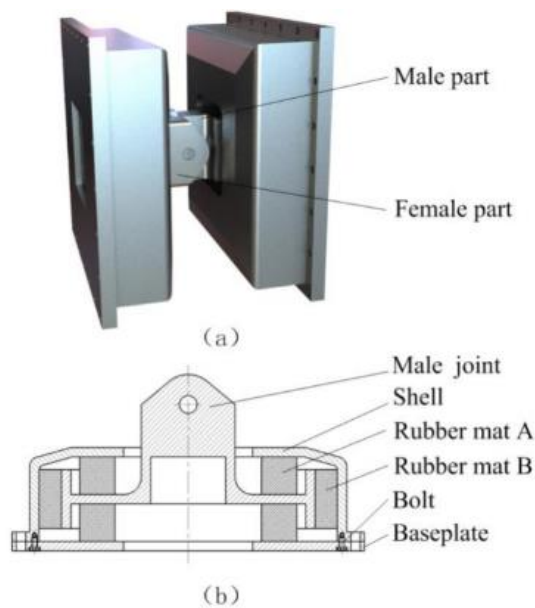


**Figure 2.7** flexible connection with the combination of steel and rubber material

For a connector system, the strength and stiffness are equally important [11]. Strength affects the structural integrity, and the stiffness determines the dynamical properties of the system.

A modularized platform is studied in the article by Ye et al. [12] consist of multiple floating modules and huge operating decks. The upper deck is hollow and internal space can be used for storages. The modules are connected using flexible connections, upper decks connected using hinge connection and upper deck connected to modules using rubber pads.

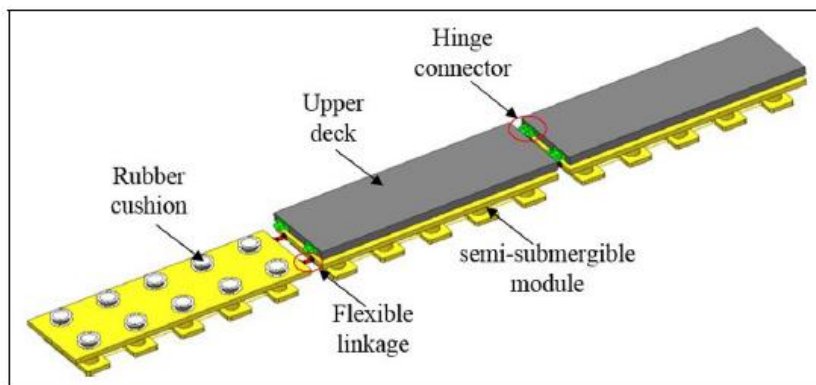


*Figure 2.8 multiple floating modules with operating decks*

Figure 2.9 shows a connecting method studied in the article [13], where concrete pontoons are connected together with a male and female shear key. The male- female shear key is advantageous in terms of construction time, cost of equipment or the working environment.

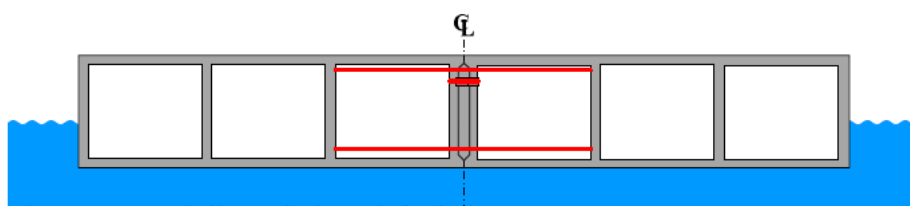


*Figure 2.9 connecting method with a male and female shear key*

Considering the current state of the art on elastic connections between platforms, no convincing solutions have been found, especially in terms of construction and implementation cost. The purpose pre-posed in this paper with the modelling of an elastic connection involves the use of a widely studied and low-cost technology: the elastomeric bearing

### 3. Elastomeric bearings

Connector of multi-modular MFI is a key component which determines the connection load and the dynamic behavior of the system. Previous attempts to develop connection systems have been proposed in the literature and the most interesting concern kinematic connections such as hinges, or elastic solutions based on the adoption of elastic and damping elements [14]. The state-of-the-art present the following limitations: lack of a comprehensive optimisation and design methodology integrated with the dynamics of MFIs, challenging engineering solutions, high costs, absence of studies concerning durability in the marine environment and maintenance. To overcome these limitations, this paper presents a new design of the flexible connection, based on elastomeric bearings that meets the requirements of flexibility, durability in marine environment, ease of connection and disconnection, and low cost.

Elastomers are an attractive material for MFI connectors as they possess excellent elastic but also shock-absorbing characteristics. The design of elastomeric bearings deals with the equilibrium between having sufficient stiffness that can withstand the imposed vertical loads and enough flexibility to allow for the expected deformations. The stiffness and flexibility requirements are well enhanced with the use of steel plates and rubber, respectively. Then, elastomeric bearings can either be plain or reinforced with internal steel plates.



*Figure 3.1 Elastomeric bearing – components*

The proper design of connector stiffness can positively affect the hydroelastic response of MFI with reduction of structural loads, and thus it represents the most significant design

parameter. Given the duration of the project, optimal stiffness values will initially be estimated by means of parametric simulations.

The functional requirements for the connection system include also: ease of connection at sea, durability in marine environment, easy decoupling procedure, able to withstand high loads.

In Figure 3.2 an example of constructive solution for the novel flexible connector is illustrated. The platforms are kept firmly together through a post-tensioning system using steel cables or rods, elastomeric bearings, and steel plates.

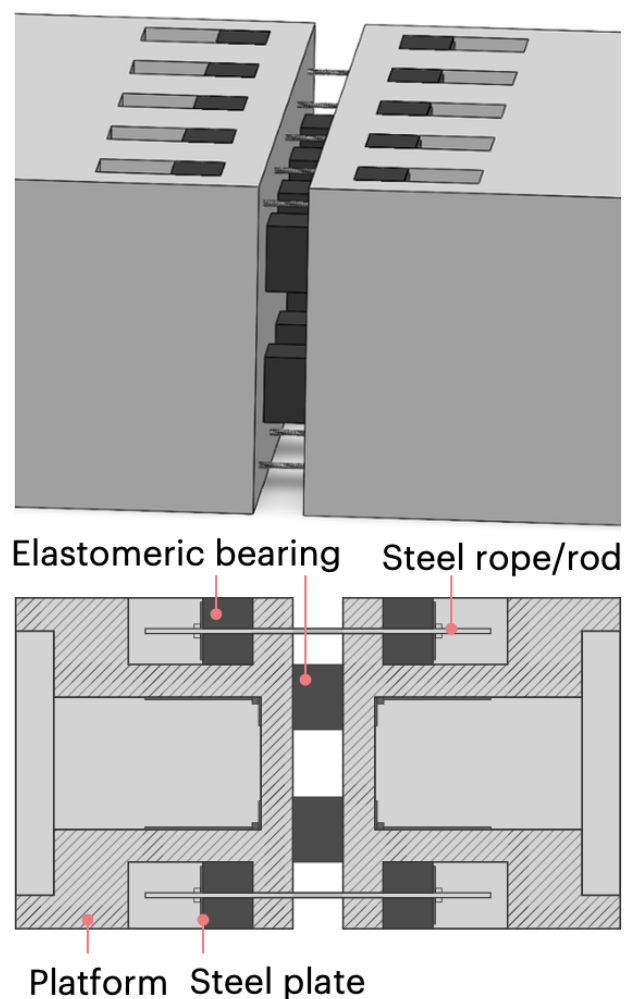


*Figure 3.2 example of constructive solution*

Elastomeric bearings are a well-known technology used principally in civil engineering [15][16] to damp vibrations and oscillations in bridges and earthquake-resistant buildings. Fender systems for port applications are another example of the use of elastomeric material

for shock attenuation of ships and pontoons at berth and demonstrate the use of this material in marine environments. In the offshore field, they are used as interface between the hull and superstructure in Floating Production Storage Offloading (FPSO) vessels [17]. The mechanical properties of elastomers combined with durability in the marine environment make this technology an excellent candidate for inter-platform connections. Experimental studies [18] have also shown the excellent fatigue behaviour of natural rubber in the presence of seawater compared to air under both relaxed and non-relaxed loading conditions [19]. The elastic characteristics depend mainly on the mechanical characteristics of the rubber and geometrical properties of the bearings. The size and type of rubber material, the presence of reinforced steel plates and lead plug are fundamental parameters of the elastomeric bearing design to guarantee the mechanical and functional requirements of the connector. Once the design requirements have been defined, different connection layouts will be studied to define the best solution.

### *3.1 Elastomeric bearings: uses and features*

The use of elastomeric bearings is becoming popular considering its well-known property of damping effect. Because of their relatively low production cost, easy installation, and good mechanical properties, they are used in civil engineering, especially in bridge construction and, more recently, as seismic isolators in buildings. But the application of these bearings is not limited to construction, it is used for the construction of joints where the damping effect is useful such as connecting of floating platforms.

Elastomeric bearings allow displacement and rotation of individual parts of the supported structure by deformation of the elastomeric material, that is, rubber. Steel-reinforced elastomeric bearings (SREB) are made by inserting steel plates between layers of rubber compound and vulcanizing this composite material [20]. The steel plates reduce the surface area of the elastomer that is free for bulging, that is, reduce the compressive deformations of the elastomer under compressive load, making the bearings stiffer. The compressive stiffness of a rubber pad is highly influenced by the shape factor  $S$ , that is, the ratio between the loaded area and the area free to bulge.

Steel plates are bonded with rubber, either natural or polychloroprene, in alternating layers to form a sandwich. The finished product contains rubber cover on the top and bottom and

around the edges, creating a sealed system in which the plates are protected against corrosion [20]. The rubber and steel layers are bonded together by an adhesive that is activated when the rubber is cured. Curing, or vulcanization, is the process of subjecting the raw rubber compound to high temperature and pressure, which both change its chemical structure and cause it to take the shape of the mold.

A plain elastomeric pad responds to vertical load by expanding laterally and slipping against the supporting surface as shown in Figure 3.3 (a). The rubber at the top and bottom surfaces of the pad is partially restrained against outward movement by friction against the support, but the rubber at mid thickness is not [20]. This results in some bulging at the edges. The lateral expansion leads to significant vertical deflections. By contrast, the rubber in the laminated pad is largely prevented from such expansion by its bond to the steel plates, and the layers only form small bulges, as shown in Figure 3.3 (b).

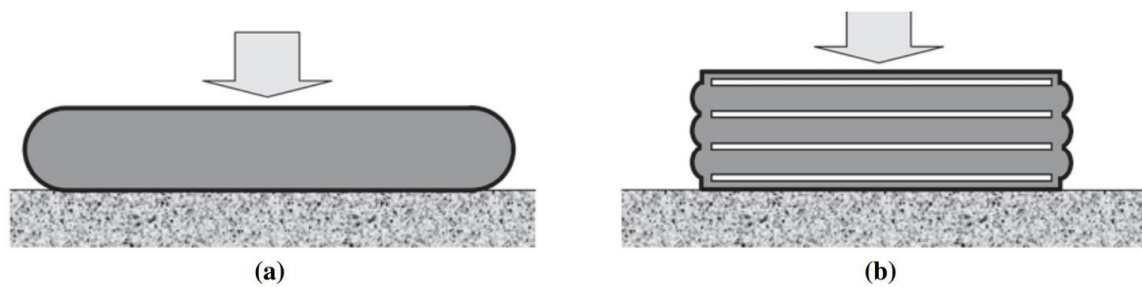


*Figure 3.3 rubber in plain (a) and laminated (b) pad*

Rubber is almost incompressible, so the volume of rubber remains almost constant under load, and the small lateral expansion leads to only a small vertical deflection. The laminated bearing is much stiffer and stronger in compression than a plain pad. However, the steel plates do not inhibit the shear deformations of the rubber, so the bearing is still able to undergo the same shear deformations as the plain pad for the purpose of accommodating changes in length of the girders [20]. Usually, these bearings are stiffer in the vertical direction and flexible in the lateral direction which enables the flexibility within the bearings.

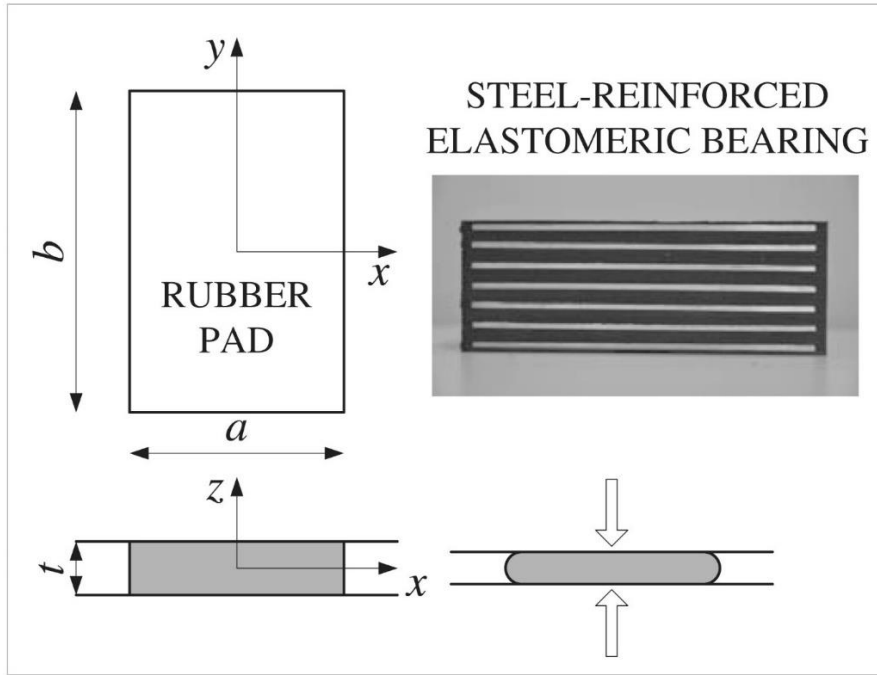


**Figure 3.4** real image of a steel-reinforced elastomeric bearing

### 3.2 Parametric modelling

The elastomeric bearings can be considered as a single link element for the structural analysis. Stiffness of this link element can be calculated given the input parameters such as dimensional properties and shear modulus.

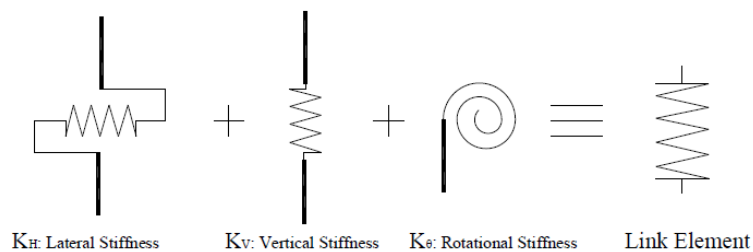


**Figure 3.5** link element

The behaviour of elastomeric material, that is, rubber under compression, is strongly influenced by different geometrical characteristics. Under compression, rubber bulges and vertical planes take up parabolic shapes. The compressive stiffness of a rubber pad is usually

related to a dimensionless parameter, the shape factor  $S$  (loaded area/area free to bulge). In this section, the compression of a rectangular rubber pad ( $a \times b \times t$ ) bonded to rigid plates is considered and the shape factor (3.1) is given by:

$$S = \frac{a b}{2 t (a + b)} \quad (3.1)$$

The Australian standard (clause 12.7) provides calculations of the stiffness of the bearings. For a rectangular cross section elastomeric bearing with certain assumptions, the simple equations can be formulated based on the Figure 3.6:

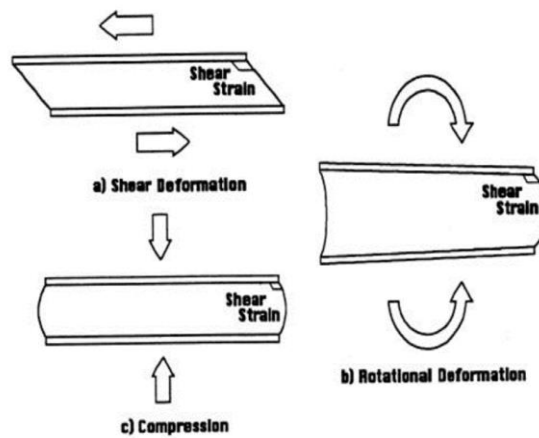


**Figure 3.6** shear, compression and rotational deformations

For the compression stiffness  $K_C$  (3.2):

$$K_c = \frac{1}{\sum_1^n \frac{1}{K_{cn}}} \quad (3.2)$$

Where,

$K_{cn} = \frac{E_c A b}{t_n}$ : compressive stiffness of an individual layer of elastomer

$E_c = 4G \left[ 1 - \left( \frac{q}{1+q^2} \right)^2 \right] + \left[ \frac{c_1 G S^2}{1 + \frac{c_1 G S^2}{0.75 B}} \right]$ : effective compression modulus of elastomer

$$C_1 = 4 + q(6 - 3.3q)$$

$q$ : minimum value of the side-to-side elastomer ratios

$G$  : elastomer shear modulus

$S$  : elastomer layer shape factor

$B$  : bulk modulus of elastomer

$A_b$ : bonded surface area

$t_n$ : thickness of a layer of elastomer

For the shear stiffness  $K_s$  (3.3):

$$K_s = \frac{A_r G}{t} \quad (3.3)$$

Where,

$A_r$ : average rubber layer plan area

$t$  : total thickness of elastomer in bearing

For the rotational stiffness  $K_r$  (3.4):

$$K_r = \frac{1}{\sum_1^n \frac{1}{K_{rn}}} \quad (3.4)$$

Where,

$K_{rn} = \frac{E_r l}{t_n}$  : compressive stiffness of an individual layer of elastomer

$E_r = 4G \left[ 1 - \left( \frac{m}{1+m^2} \right)^2 \right] + \left[ \frac{C_2 G S^2}{1 + \frac{C_2 C^2}{0.758}} \right]$  effective compression modulus of elastomer

$$C_2 = 4 - \frac{32}{10+m(4+3m+m^2)}$$

$m$ : parallel-to-transverse side of span elastomer dimension ratio for rotation about an axis parallel to the long dimension of the bearing

$I$ : Moment of inertia about the axis of rotation

To account for the compressibility of rubber, it is necessary to accurately estimate the material's resistance to volume change under compression, that is, the value of the bulk modulus of rubber. According to the European standard EN 1337-3, typical rubber used for

SREBs is carbon-filled rubber with a hardness of 60 IRHD (International Rubber Hardness Degree), elastomer shear modulus  $G = 0.9$  MPa and bulk modulus  $B = 2000$  MPa.

### *3.3 Stiffness and geometrical parameters*

The effect of the variation of the construction parameters of the bearings on axial, lateral and bending stiffness was analysed. In particular, the shape of bearings selected is square, since those are the ones that are most easily found on the market.

It can clearly be observed from Figure 3.7 that increasing the number of layers, and consequently the overall height of the bearing, leads to a reduction of the compression stiffness. The trend observed is characteristic of springs positioned in series, adding layers of rubber in fact is equivalent to adding stiffnesses one above the other, this results into a reduction in the overall stiffness. The magnitude in the reduction in axial stiffness decreases as the number of elastomer layers increases; in fact, the most significant reduction occurs when going from a bearing with only one elastomer layer to one with 2 layers.

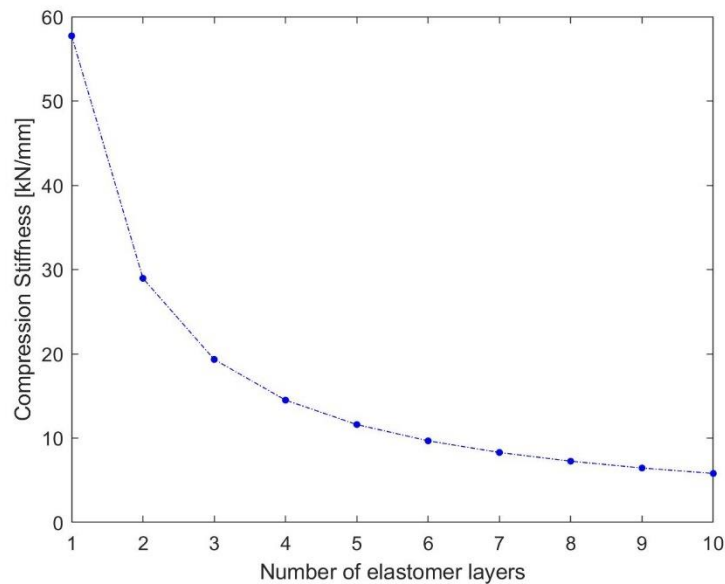


**Figure 3.7** *compression stiffness for variable number of elastomer layers*

It can be observed from Figure 3.8 that increasing the number of layers, and consequently the overall height of the bearing, leads to a reduction of lateral stiffness. It is also noted that the value of the lateral stiffness is an order of magnitude less than that of the axial stiffness; this is a fundamentally important observation, as this value of stiffness could be a limiting factor in the sizing of the connection due to its small magnitude. Just as observed in the case of axial stiffness, again the most significant reduction is observed in the transition from the 1-layer elastomer configuration to the 2-layer configuration.

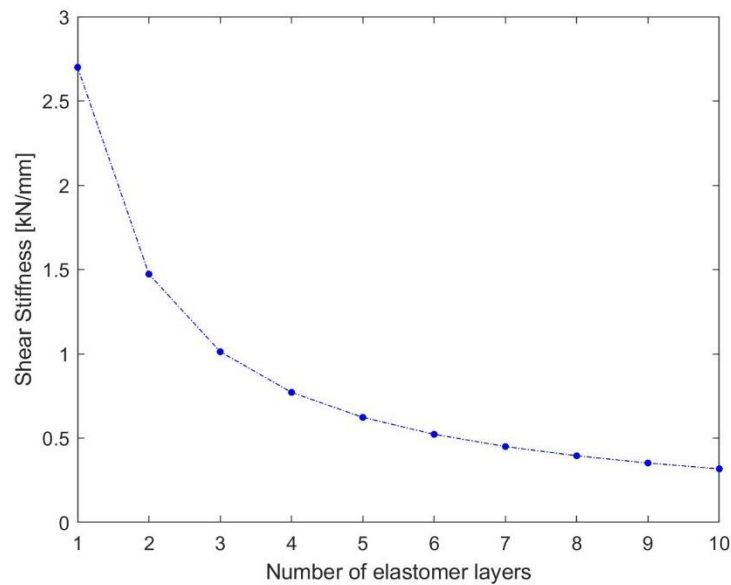


**Figure 3.8** shear stiffness for variable number of elastomer layers

The increase in the rubber surface leads to an increase in axial stiffness (Figure 3.9), this is clearly due to the fact that the increase in the size results in an increase in the form factor, directly proportional to the stiffness of the bearings. The increase in axial stiffness is not linear with elastomer size but has a clearly quadratic trend; this is something that will have to be particularly taken into account when sizing the connection, since small changes in size correspond to high changes in stiffness.

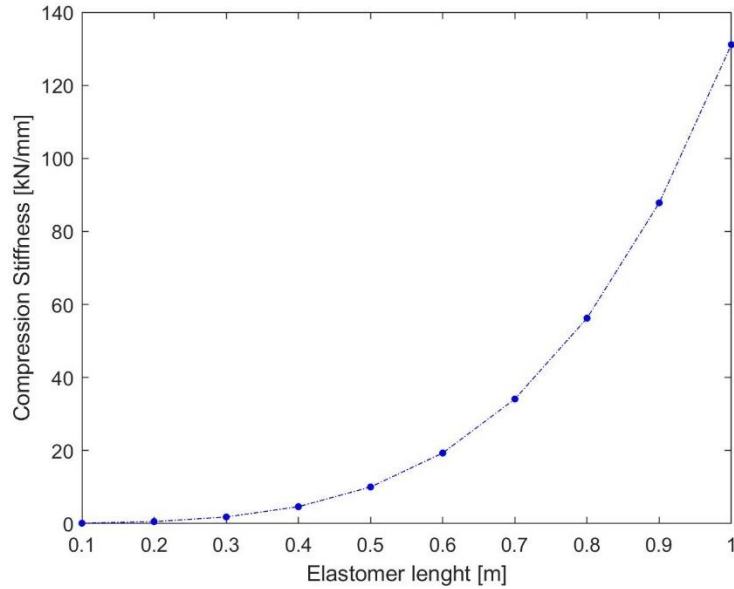


**Figure 3.9** compression stiffness for variable elastomer length

The increase in the rubber surface leads to an increase in shear stiffness (Figure 3.10), this is clearly due to the fact that the increase in the size results in an increase of the average rubber layer plan, directly proportional to the shear stiffness of the bearings. The increase in shear stiffness is not linear with elastomer size but has a quadratic trend; but the range of stiffnesses available is very much reduced if compared with the one of the compression stiffness.

The stiffness of elastomeric bearings is largely influenced by the ratio of height to the area of the bearing and the number of laminated reinforcing plates. The elastomeric bearings of the same size may have different stiffnesses depending on the number of reinforcing plates inserted into the elastomer.

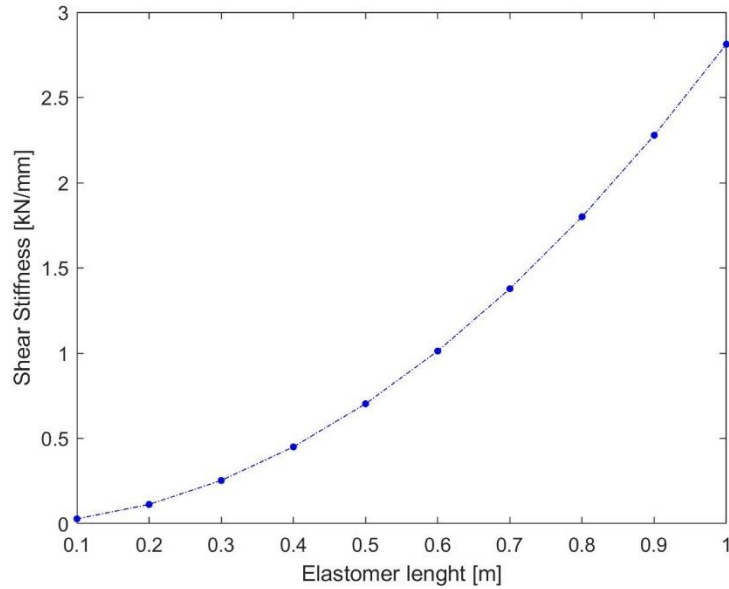


**Figure 3.10** lateral stiffness for variable elastomer length

To analyse the effect of the reinforcing plate on the compression and shear of an  $600 \times 600 \times 300$  mm elastomeric bearing was selected as the target model. The number of reinforcing plates (Ns) was selected as a design parameter, and a total of 9 models with 0 to 8 reinforcing plates with 5 mm thickness were selected as analysis models.

For the same size and overall bearing height, a substantial increase in axial stiffness is observed as the number of reinforcing steel plates increases (Figure 3.11). The steel plates reduce the surface area of the elastomer that is free for bulging, that is, reduce the compressive deformations of the elastomer under compressive load, making the bearings stiffer. It is also noted that the increase in stiffness is Greater as the number of steel plates used increases.

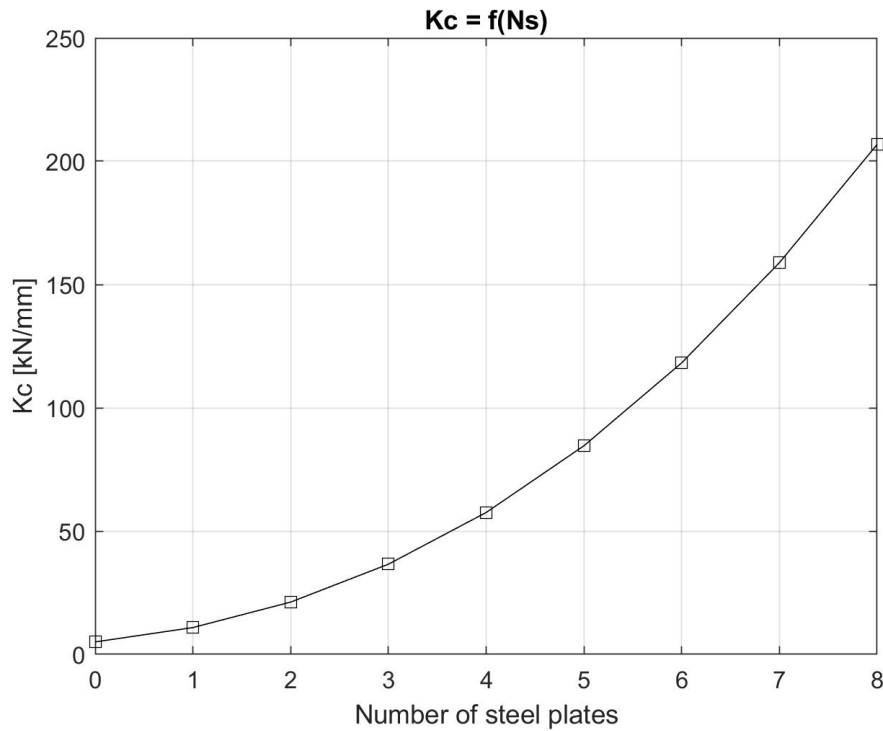


**Figure 3.11** axial stiffness for variable number of steel reinforcing plates

Overall, the influence of the number of reinforcing plates (Ns) on the shear stiffness of the elastomeric bearing is small (Figure 3.12). It is observed that the addition of reinforcing steel layers does not have a major impact on the lateral stiffness if the total elastomeric thickness remains the same. In fact, the steel plates do not inhibit the shear deformations of the rubber, so the bearing is still able to undergo the same shear deformations as the plain pad.

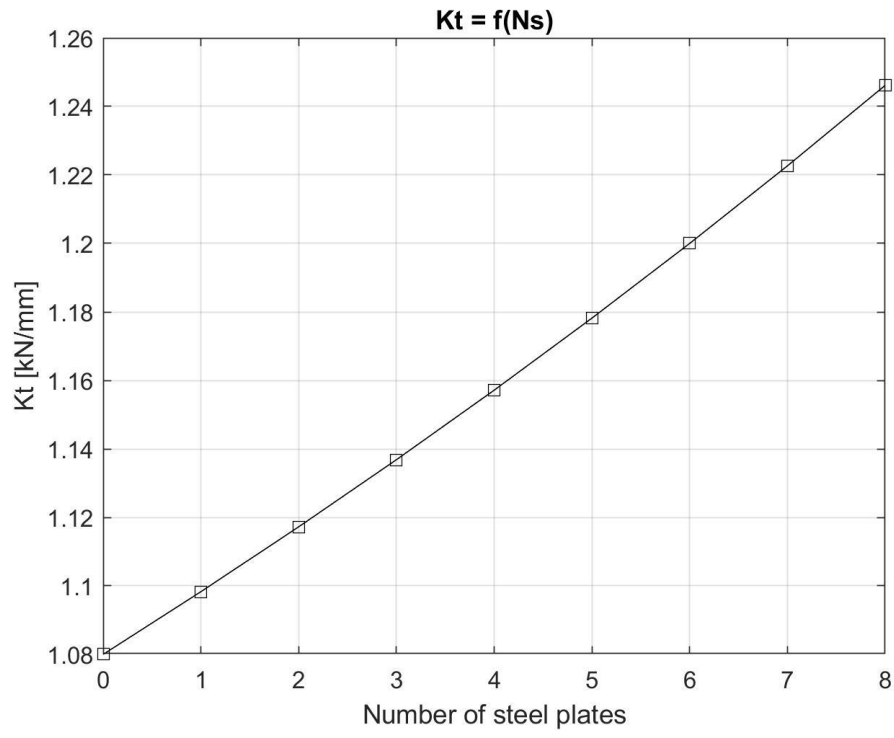


**Figure 3.12** lateral stiffness for variable number of steel reinforcing plates

## 4. Dynamics of multibody system

The work presented in this chapter focuses on the optimization of the connection stiffness of modular hexagonal floating islands. The connection system is described by an equivalent system consisting of linear springs whose stiffness is the objective of optimization. The aim is to find an optimal spring stiffness solution (unique for the different island configurations) that is compliant with dynamic constraints of human comfort and that minimizes the loads acting on the connections.

The methodology developed in this work can be applied for various geometries and sizes of floating platforms and can be extended for a different number of connected devices. A hexagonal platform geometry was chosen for the analysis, as this allows for honeycomb layouts for greater freedom of shape of the floating island. In addition, the hexagonal shape allows for a better spatial distribution of the connection forces, compared to the square geometry case.

Acceptable human comfort values of accelerations and displacements, required by structures for residential purposes, pose new and unique challenges for the design of MFIs and plays a significant role in the design feasibility. The system will be simulated both in regular and irregular waves.

### *4.1 Connector stiffness matrix*

In general, a multibody system is defined to be a collection of subsystems called bodies, components, or substructures [21]. The motion of the subsystems is kinematically constrained because of different types of joints, and each subsystem or component may undergo large translations and rotational displacements. Basic to any presentation of multibody mechanics is the understanding of the motion of subsystems (bodies or components). The multibody system consists of interconnected rigid and deformable bodies, each of which may undergo large translational and rotational displacements [21].

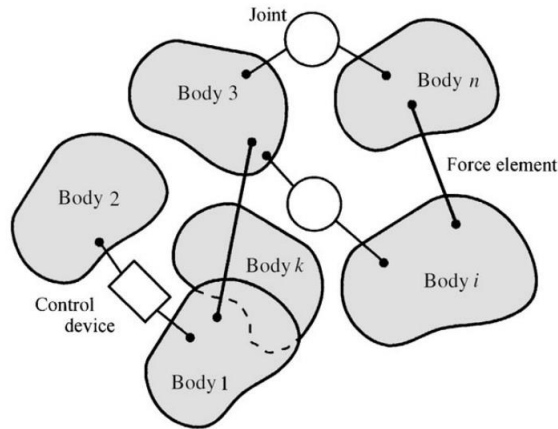


**Figure 4.1** example of multibody system

Many mechanical and structural systems such as vehicles, space structures, robotics, mechanisms, and aircraft consist of interconnected components that undergo large translational and rotational displacements.

The term rigid body implies that the deformation of the body under consideration is assumed small such that the body deformation has no effect on the gross body motion. Hence, for a rigid body, the distance between any two of its particles remains constant at all times and all configurations [21]. The motion of a rigid body in space can be completely described by using six generalized coordinates, but the problem has been approached in a plane system in which each body has three degrees of freedom: surge, heave, and pitch.

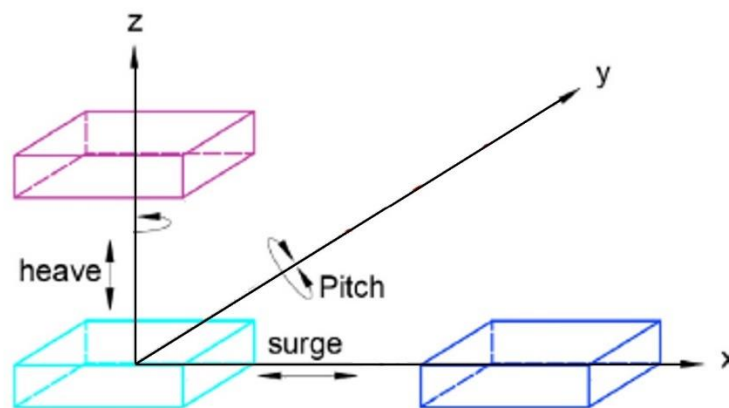


**Figure 4.2** surge, heave and pitch motions

The configuration of a multibody system can be described using measurable quantities such as displacements, velocities, and accelerations. These are vector quantities that have to be measured with respect to a proper frame of reference or coordinate system. Generally, in dealing with multibody systems two types of coordinate systems are required. The first is a coordinate system that is fixed in time and represents a unique standard for all bodies in the system. This coordinate system will be referred to as global, or inertial frame of reference. In addition to this inertial frame of reference, a body reference to each component in the system is assigned, for example  $x_1z_1$  for the first body, his body reference translates and rotates with the body; therefore, its location and orientation with respect to the inertial frame change with time. The position of the global reference  $XZ$  is defined, and the position of inertial frames of reference to each component in the system, for example  $X_1Z_1$  for the first body (Figure 4.3).

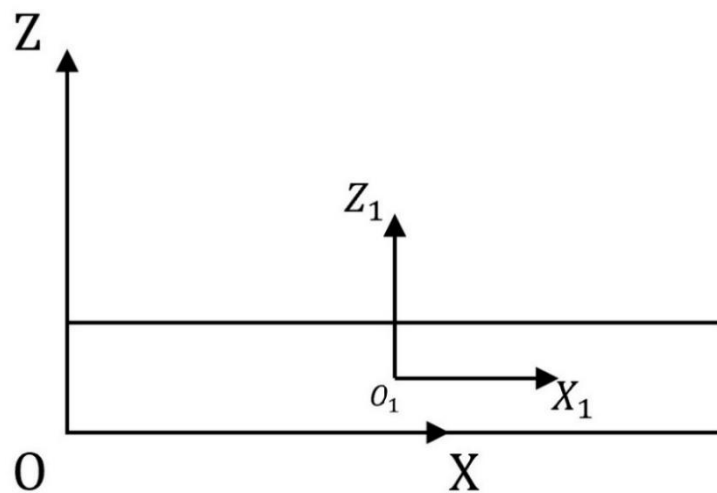


*Figure 4.3 frames of reference*

The connection system is represented by a system of equivalent linear springs as shown in the Figure 4.4. The layout of the connection ensures a certain degree of rigidity between the platforms by acting on the surge, heave, and pitch degrees of freedom. These hypotheses allow us to better highlight the effect of the stiffness of the connections on the dynamics of interconnected floating platforms under the action of sea waves. Future work will expand the model to consider the three-dimensional effects of the connections on the various sides of the hexagon in various configurations.

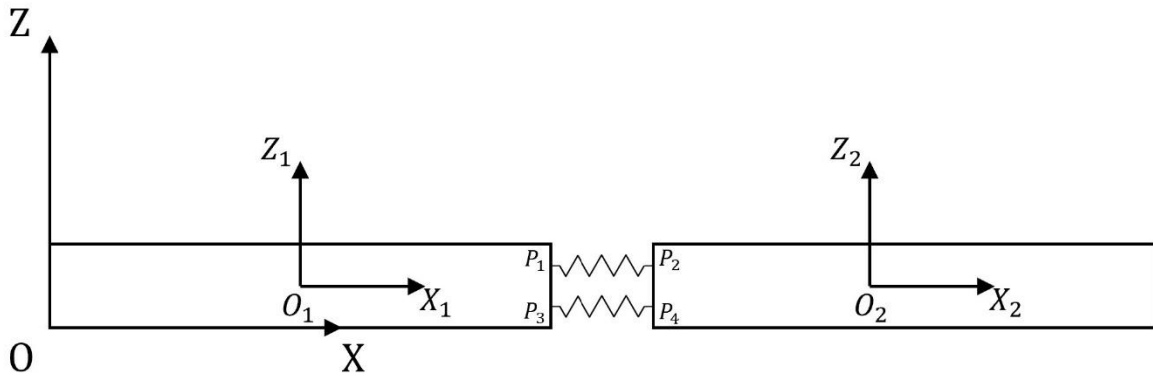


**Figure 4.4** equivalent linear springs

Although the study has been conducted for only two platforms it is of general value, since it can be easily extended, in the linear case, to multiple bodies by manipulation of the stiffness matrix.

The points designated as “P” are the anchor points between elastomers and platforms, through these points the transmission of forces between the platforms takes place; it follows that the distances  $\overline{P_1P_2}$  and  $\overline{P_3P_4}$  are of fundamental importance for the study of the system. This distance depends on surge, heave, and pitch motion of the individual platforms, for the  $i$ th platform those quantities are identified respectively as  $\theta_i$ ,  $x_i$  and  $z_i$  (Figure 4.5).

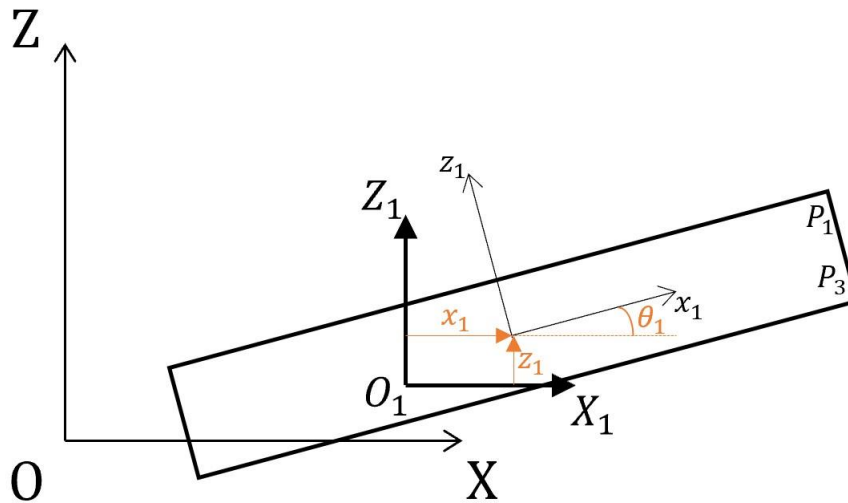


**Figure 4.5** surge, heave, and pitch motion of the individual platform

The dimensions of the floating structure under investigation are shown in the table 4.1. The small size of the platform is motivated by the fact that a 1:3 scale prototype is being developed to be installed in a protected site for experimental purposes. As the numerical

model adopted is linear, the results obtained here can be scaled up to assess the effects on the system at full scale.

Dimensions	Description	Value
a	distance between elastomer application point and centre of the connection	1.2 m
D	diameter of the circumference circumscribed by the hexagonal platform	18 m
b	apothem of the hexagonal platform	7,8 m
H	hight of the platform	3 m
$l_0$	length of the elastomer at rest	0.5 m

*Table 4-1 platform dimensions*

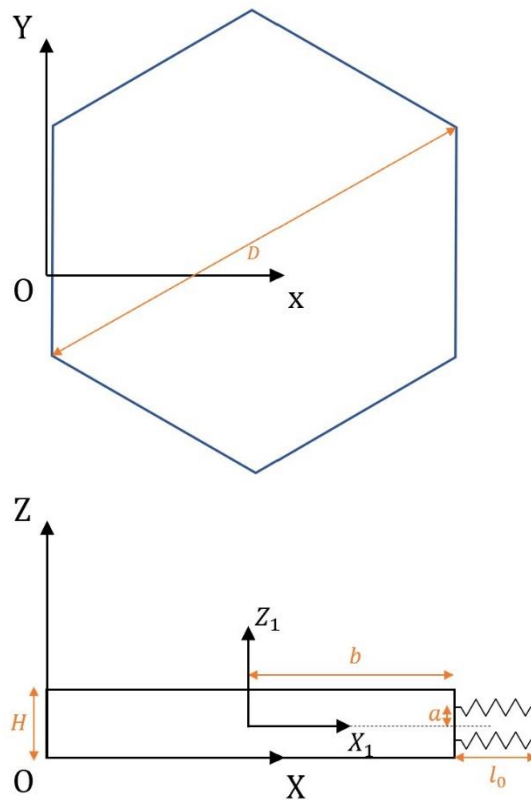


*Figure 4.6 main dimensions of the platform*

The position of each point is derived, with respect to the local inertial frame of reference  $X_iZ_i$  first and then with respect to the global reference system  $XZ$ .

$$\overline{O_1P_1} = \begin{cases} x_1 + b \cos \theta_1 - a \sin \theta_1 \\ z_1 + b \sin \theta_1 + a \cos \theta_1 \end{cases}$$

$$\overline{O_2P_2} = \begin{cases} x_2 - b \cos \theta_2 - a \sin \theta_2 \\ z_2 + b \sin \theta_2 + a \cos \theta_2 \end{cases}$$

$$\overline{OP_1} = \begin{cases} x_1 + b \cos \theta_1 - a \sin \theta_1 + b \\ z_1 + b \sin \theta_1 + a \cos \theta_1 + \frac{H}{2} \end{cases}$$

$$\overline{OP_2} = \begin{cases} x_2 - b \cos \theta_2 - a \sin \theta_2 + 3b + l_0 \\ z_2 + b \sin \theta_1 + a \cos \theta_1 + \frac{H}{2} \end{cases}$$

$$\overline{O_1P_3} = \begin{cases} x_1 + b \cos \theta_1 + a \sin \theta_1 \\ z_1 + b \sin \theta_1 - a \cos \theta_1 \end{cases}$$

$$\overline{O_2P_4} = \begin{cases} x_2 - b \cos \theta_2 + a \sin \theta_2 \\ z_2 - b \sin \theta_2 - a \cos \theta_2 \end{cases}$$

$$\overline{OP_3} = \begin{cases} x_1 + b \cos \theta_1 + a \sin \theta_1 + b \\ z_1 + b \sin \theta_1 - a \cos \theta_1 + \frac{H}{2} \end{cases}$$

$$\overline{OP_4} = \begin{cases} x_2 - b \cos \theta_2 + a \sin \theta_2 + 3b + l_0 \\ z_2 - b \sin \theta_2 - a \cos \theta_2 + \frac{H}{2} \end{cases}$$

The mechanical behaviour of the connection system is represented by an equivalent system of two linear springs (see Figure 4.7) that constraint respectively the relative surge, heave, and pitch motion of adjacent platforms.

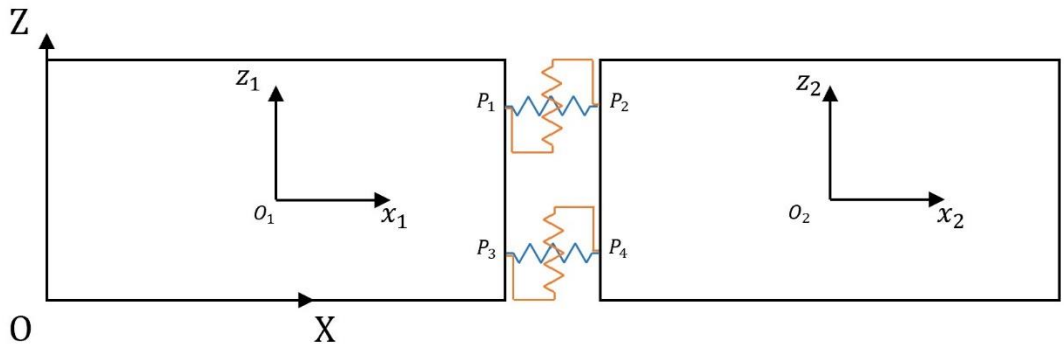


**Figure 4.7** equivalent system of two linear springs

Given this schematization, it is possible to derive the elastomer shortening in the x-direction and z-direction for both connections:

$$\Delta x_{P_1P_2} = \overline{OP_{2(x)}} - \overline{OP_{1(x)}} = 2b - b(\cos \theta_2 + \cos \theta_1) + a(\sin \theta_1 - \sin \theta_2) + x_2 - x_1$$

$$\Delta z_{P_1P_2} = \overline{OP_{2(z)}} - \overline{OP_{1(z)}} = -b(\sin \theta_2 + \sin \theta_1) + a(\cos \theta_2 - \cos \theta_1) + z_2 - z_1$$

$$\Delta x_{P_3P_4} = \overline{OP_{2(x)}} - \overline{OP_{1(x)}} = 2b - b(\cos \theta_2 + \cos \theta_1) + a(\sin \theta_2 - \sin \theta_1) + x_2 - x_1$$

$$\Delta z_{P_3P_4} = \overline{OP_{2(z)}} - \overline{OP_{1(z)}} = -b(\sin \theta_2 - \sin \theta_1) + a(\cos \theta_2 - \cos \theta_1) + z_2 - z_1$$

A simplification, valid in the case of small oscillations as the one considered in this work, is applied at this stage: this consists in confusing the axial and lateral stiffness of the elastomer as the stiffnesses along x and along z, respectively. This is a simplification since in reality in the presence of non-zero platform pitch the axial direction of the elastomer will no longer coincide with the “x” direction but will be slightly different. However, for small pitch angles this difference can be neglected. The forces acting along x(4.1) and z(4.2) will therefore be:

$$F_x = K_x(\Delta x_{P_1P_2} + \Delta x_{P_3P_4}) \quad (4.1)$$

$$F_z = K_z(\Delta z_{P_1P_2} + \Delta z_{P_3P_4}) \quad (4.2)$$

From the deformations, not only the forces exchanged but also the elastic potential energy for each connection is calculated. It is observed that for each connection the elastic energy is composed of two terms, one involving the deformation along x(4.3) and the other along z(4.4).

$$U_{e_{1-2}} = \frac{1}{2}(K_x (\Delta x_{P_1P_2})^2 + K_z (\Delta z_{P_1P_2})^2) \quad (4.3)$$

$$U_{e_{3-4}} = \frac{1}{2}(K_x (\Delta x_{P_3P_4})^2 + K_z (\Delta z_{P_3P_4})^2) \quad (4.4)$$

At this point in order to apply Hamilton's law, the spatial derivative of the elastic potential energy is calculated, with respect to each degree of freedom:

For the connection between platforms 1 - 2:

$$\frac{\partial U_{e_{1-2}}}{\partial x_1} = -K_x(\Delta x_{P_1P_2}) - K_z(\Delta z_{P_1P_2})$$

$$\frac{\partial U_{e_{1-2}}}{\partial x_2} = K_x(\Delta x_{P_1P_2}) + K_z(\Delta z_{P_1P_2})$$

$$\frac{\partial U_{e_{1-2}}}{\partial \theta_1} = K_x(\Delta x_{P_1P_2})(b \sin \theta_1 + a \cos \theta_1) + K_z(\Delta z_{P_1P_2})(-b \cos \theta_1 + a \sin \theta_1)$$

$$\frac{\partial U_{e_{1-2}}}{\partial \theta_2} = K_x(\Delta x_{P_1P_2})(b \sin \theta_2 - a \cos \theta_2) + K_z(\Delta z_{P_1P_2})(-a \sin \theta_2 - b \cos \theta_2)$$

For the connection between platforms 2 - 3:

$$\frac{\partial U_{e_{3-4}}}{\partial x_1} = -K_x(\Delta x_{P_3P_4}) - K_z(\Delta z_{P_3P_4})$$

$$\frac{\partial U_{e_{3-4}}}{\partial x_2} = K_x(\Delta x_{P_3P_4}) + K_z(\Delta z_{P_3P_4})$$

$$\frac{\partial U_{e_{3-4}}}{\partial \theta_1} = K_x(\Delta x_{P_3P_4})(b \sin \theta_1 - a \cos \theta_1) + K_z(\Delta z_{P_3P_4})(-b \cos \theta_1 - a \sin \theta_1)$$

$$\frac{\partial U_{e_{3-4}}}{\partial \theta_2} = K_x(\Delta x_{P_3P_4})(b \sin \theta_2 + a \cos \theta_2) + K_z(\Delta z_{P_3P_4})(a \sin \theta_2 - b \cos \theta_2)$$

The equations derived are clearly nonlinear, since it's interest of this work a qualitative calculation, designed to verify that the forces and deformations involved allow the usage of elastomeric bearing to construct the link between the platforms, and since low pitch values are expected, the assumption of linearity is made, simplifying as:

$$\sin \theta \approx \theta ;$$

$$\cos \theta \approx 1;$$

Substituting gives:

$$\frac{\partial U_{e_{1-2}}}{\partial x_1} \approx -K_x(a \theta_1 - a \theta_2 + x_2 - x_1) - K_z(-b \theta_1 - b \theta_2 + z_2 - z_1)$$

$$\frac{\partial U_{e_{1-2}}}{\partial x_2} = K_x(a \theta_1 - a \theta_2 + x_2 - x_1) + K_z(-b \theta_1 - b \theta_2 + z_2 - z_1)$$

$$\frac{\partial U_{e_{1-2}}}{\partial \theta_1} = K_x(a^2 \theta_1 - a^2 \theta_2 + a x_2 - a x_1) + K_z(b^2 \theta_1 + b^2 \theta_2 - b z_2 + b z_1)$$

$$\frac{\partial U_{e_{1-2}}}{\partial \theta_2} = K_x(-a^2 \theta_1 + a^2 \theta_2 - a x_2 + a x_1) + K_z(b^2 \theta_1 + b^2 \theta_2 - b z_2 + b z_1)$$

Doing the same for  $U_{e_{3-4}}$ , the values of the linearized spatial derivatives are obtained. At this point the Hamilton's theorem is applied, for which, from the value of the spatial derivatives the stiffness matrices of the system are derived. The stiffness matrices  $[K_x]$ (4.5) and  $[K_z]$ (4.6) can be written as:

$$[K_z] = -2 K_z \begin{bmatrix} 1 & b & -1 & b \\ b & b^2 & -b & b^2 \\ -1 & -b & 1 & -b \\ b & b^2 & -b & b^2 \end{bmatrix} \quad (4.5)$$

$$[K_x] = -2 K_x \begin{bmatrix} 1 & 0 & -1 & 0 \\ 0 & a^2 & 0 & -a^2 \\ -1 & 0 & 1 & 0 \\ 0 & -a^2 & 0 & a^2 \end{bmatrix} \quad (4.6)$$

And the overall stiffness matrix (4.7):

$$[K] = -2 \begin{bmatrix} K_x & 0 & 0 & -K_x & 0 & 0 \\ 0 & K_z & b K_z & 0 & -K_z & b K_z \\ 0 & b K_z & a^2 K_x + b^2 K_z & 0 & -b K_z & -a^2 K_x + b^2 K_z \\ -K_x & 0 & 0 & K_x & 0 & 0 \\ 0 & -K_z & -b K_z & 0 & K_z & -b K_z \\ 0 & b K_z & -a^2 K_x + b^2 K_z & 0 & -b K_z & a^2 K_x \end{bmatrix} \quad (4.7)$$

At this stage the main goal of the analysis is achieved, which is to derive a stiffness matrix that can be implemented in the numerical model of the system to perform the simulations, in order to observe the behaviour of the system as the stiffnesses changes and as the sea state changes. However, the result of the multibody analysis satisfies us only in part; in fact, it is our intention to simulate the behaviour of three interconnected platforms. From the result obtained, however, it is possible to get the stiffness matrix of a system consisting of any number of interconnected platforms by applying a linear combination of the matrices. Thus, the stiffness matrix for three interconnected platforms (4.8) is derived.

$$[K] = -2 \begin{bmatrix} K_x & 0 & 0 & -K_x & 0 & 0 & 0 & 0 & 0 \\ 0 & K_z & b K_z & 0 & -K_z & b K_z & 0 & 0 & 0 \\ 0 & b K_z & a^2 K_x + b^2 K_z & 0 & -b K_z & -a^2 K_x + b^2 K_z & 0 & 0 & 0 \\ -K_x & 0 & 0 & 2 K_x & 0 & 0 & -K_x & 0 & 0 \\ 0 & -K_z & -b K_z & 0 & 2 K_z & 0 & 0 & -K_z & b K_z \\ 0 & b K_z & -a^2 K_x + b^2 K_z & 0 & 0 & 2 (a^2 K_x + b^2 K_z) & 0 & -b K_z & -a^2 K_x + b^2 K_z \\ 0 & 0 & 0 & -K_x & 0 & 0 & K_x & 0 & 0 \\ 0 & 0 & 0 & 0 & -K_z & -b K_z & 0 & K_z & -b K_z \\ 0 & 0 & 0 & 0 & b K_z & -a^2 K_x + b^2 K_z & 0 & -b K_z & a^2 K_x + b^2 K_z \end{bmatrix} \quad (4.8)$$

From the analysis of the stiffness matrix, it can be observed how the different quantities are related to each other, for example how the pitching moment is strongly related to the size of the platform and the positioning of the elastomer.

#### *4.2 Regular wave analysis*

Within this framework, linear three-dimensional potential flow theory will be used to calculate the hydrodynamic forces. This theory assumes incompressible fluid and irrotational and inviscid flow. The 3-D Boundary Element Method (BEM) open-source software Nemoh [22] is adopted to compute the hydrodynamic frequency domain coefficients. BEM codes solve the interaction problem between multiple floating bodies by considering all bodies as part of the boundary value problem (BVP) for the calculation of the potential flow solution. In this preliminary work the influence of the mooring system will

be neglected and only the surge, heave and pitch motion of each platform is considered in the analysis to simplify the analysis. Figure 4.8 shows the global and body reference system of the case study under analysis, that consists of three hexagonal floating platforms arranged in a line.

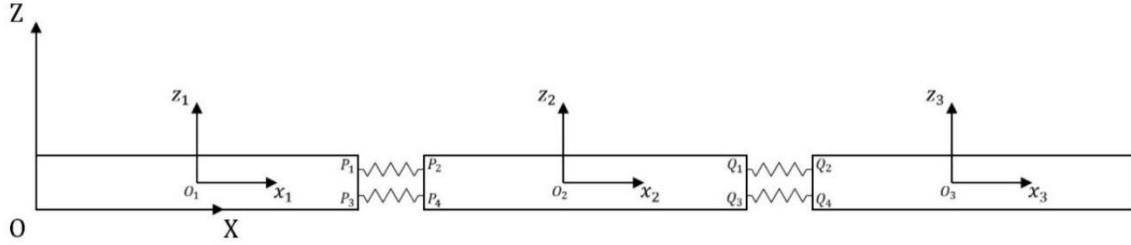


**Figure 4.8** global and body reference system

The mesh of the system has been calculated with SALOME-MECA tool and it is illustrated in figure 4.9.

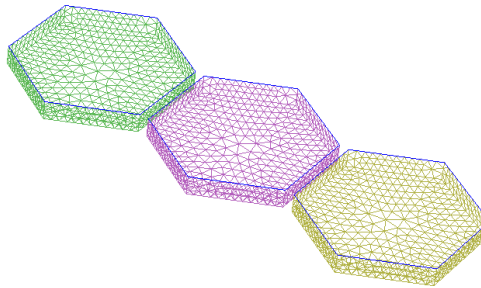


**Figure 4.9** mesh of the system

In this case study only the surge, heave, and pitch degree of freedoms (4.9) of the three floating bodies are considered, and thus the state variable vector  $X$  has dimension 9:

$$X = [x_1, z_1, \delta_1, x_2, z_2, \delta_2, x_3, z_3, \delta_3] \quad (4.9)$$

Solving the BEM problem makes it possible to calculate the frequency-dependent hydrodynamic coefficients and thus to define the equations describing the dynamics of the multibody system in the frequency domain (4.10):

$$[-\omega^2(M + A(\omega)) + i\omega B(\omega) + (K_h + K_c)]X(\omega) = F_{ext}(\omega) \quad (4.10)$$

Where  $M$  is the structural inertia,  $A$  is the added mass,  $B$  is the linear radiation damping,  $K_h$  is the hydrostatic stiffness,  $K_c$  is the linearised stiffness matrix of the connection system and  $F_{ext}$  is the excitation force coefficients vector and is directly proportional to the wave amplitude  $a$ . The mathematical derivation of the stiffness matrix due to connections will be addressed in the next section. From equation (4.10) is possible to define the frequency dependent Response Amplitude Operator (RAO)(4.11) of the entire multi-body floating system:

$$RAO(\omega) = \frac{X(\omega)}{a} = \frac{f(\omega)}{[-\omega^2(M + A(\omega)) + i\omega B(\omega) + (K_h + K_c)]} \quad (4.11)$$

Within this modelling framework, we preliminarily neglect the effects of second order forcing, the average force components due to waves, currents, and wind, and consider long crested waves without directional spreading. Concerning the modelling of irregular waves, in this work we refer to the analytical spectrum of Jonswap considering a peak enhancement factor  $\gamma = 3.3$ . Since the numerical model is linear, it is possible to calculate the Power Spectral Density (PSD) of the system state variables  $S_X(\omega)$ , given the RAO of the system and the wave PSD  $S_\eta(\omega)$ :

$$S_X(\omega) = |RAO(\omega)|^2 S_\eta(\omega)$$

Given the PSD of the state variables it is possible to compute their expected RMS value  $RMS_X$  (equivalent to the standard deviation  $\sigma_X$  of the statistical process). Since the input wave is assumed to be a Gaussian process, thus also the output is Gaussian. Thus, we consider as maximum value of the process  $X_{max} = 3 \cdot \sigma_X$ , that includes 99.73% of the probability of the Gaussian process.

The first simulations are the ones in regular wave, these were performed by simulating on the Matlab platform sine waves of constant amplitude and phases. The RAO was calculated for different values of the system, including elastomer deformation in x and z direction, pitching of individual platforms, and forces exchanged between platforms.

Looking at the Figure 4.10, it can be observed that in for each platform motion analysed there is a different displacement of the isolated platform compared to the three platforms

when placed together in the sea, in particular the pitch motion is reduced for each wave period considering the three platforms.

A further observation that can be made by looking at the graphs is that the first platform has a much more pronounced motion than that of the other platforms, this is due to the fact that the first platform is the first to be hit by the wave, the other two platforms are therefore shielded from it and for this reason a reduced motion is observed.

Finally, it can be observed that the maximum pitching motion occurs for different wave periods among the platforms, around 5 s in the case of the first platform as well as for the single platform, and for increasing wave periods for the other platforms, up to a maximum of about 6 s for the third platform.

The motion of the isolated platform is compared with the other platforms when connected to each other via the elastomeric connection; at this stage non-optimized values of stiffnesses  $K_x$  and  $K_z$  are used, for the sole purpose of observing the effect of the connection on the motion, in particular at this stage values of 20 kN/mm and 5 kN/mm of  $K_x$  and  $K_z$  are assumed.

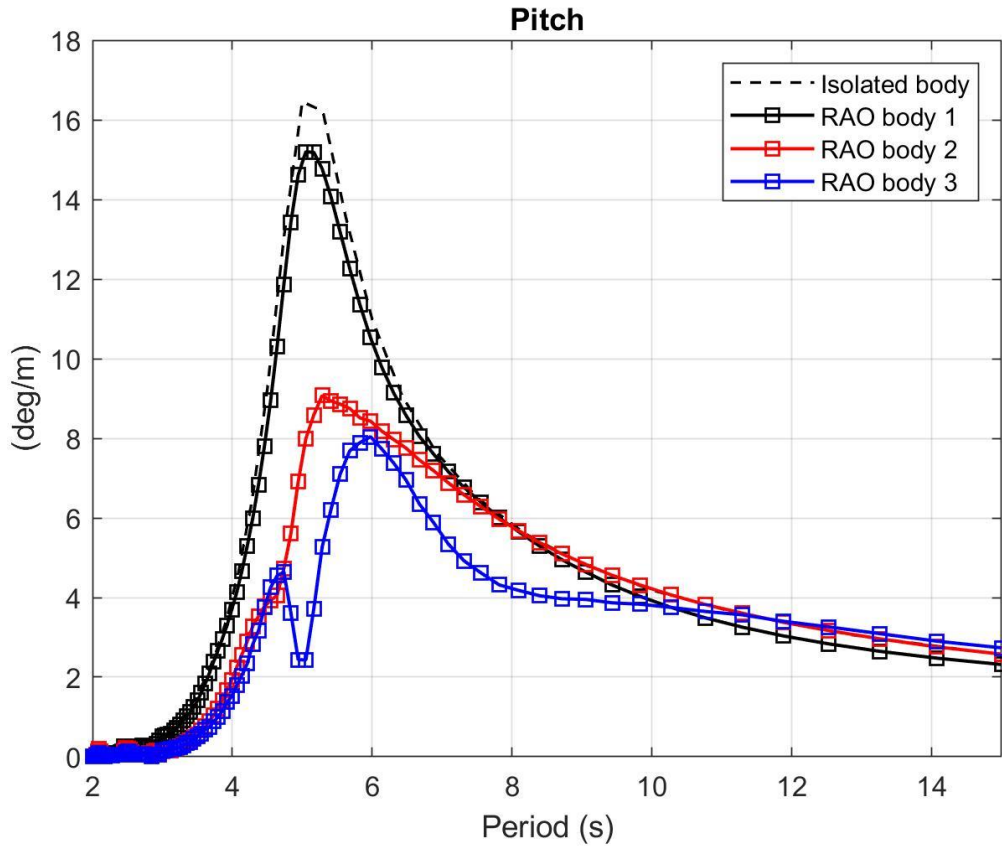


*Figure 4.10 RAO – max pitch unconnected platforms*

The addition of a connection of stiffness  $K_x = 20 \text{ kN/mm}$  and  $K_z = 5 \text{ kN/mm}$  results in a significant reduction in the pitching of the system (Figure 4.11), compared to the configuration without a connection it can be noted that the platforms pitch in unison with similar pitching values among them. A first maximum is observed for  $T = 4 \text{ s}$  and a second maximum for longer periods, this is a dynamic that is absent for individual platforms and is only observed in the presence of connection.

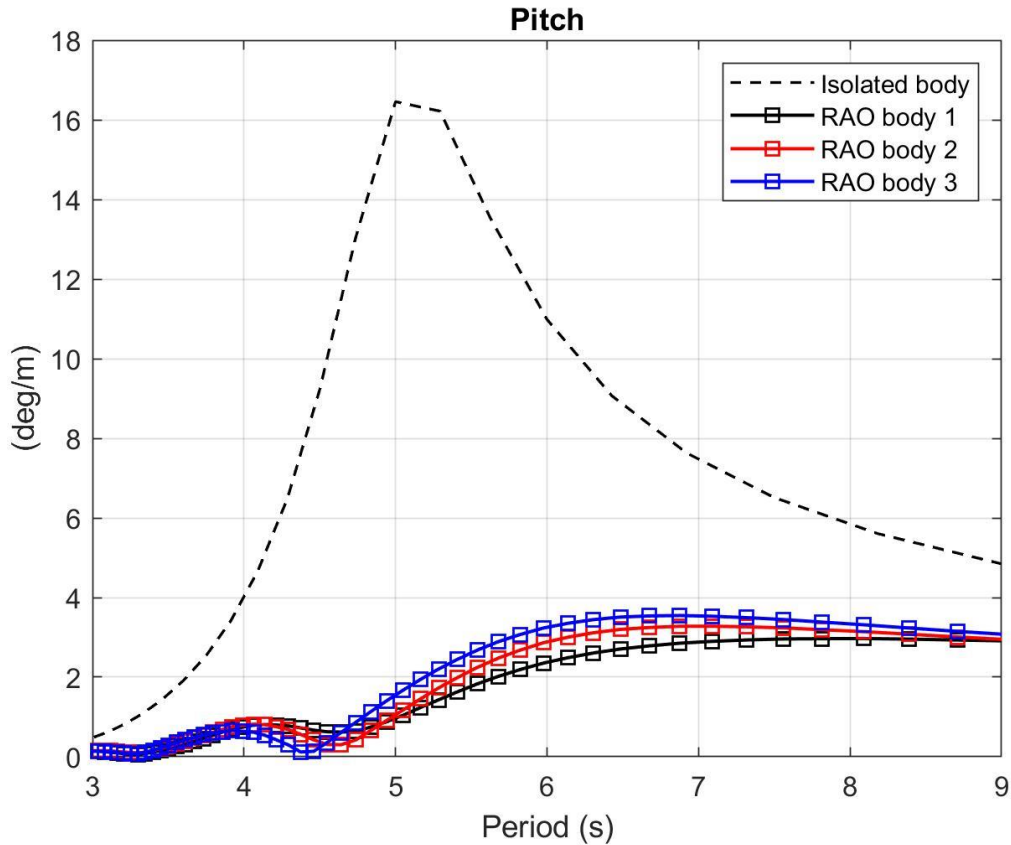


**Figure 4.11** RAO – max pitch connected platforms

It can be observed that the increase in stiffness results in a significant reduction in pitching motion for all platforms (Figure 4.12), in particular it can be observed that for the first platform there is a more gradual reduction in pitching, an indication of the fact that greater stiffnesses are required than for the other platforms for its motion to be mitigated, the second platform on the contrary undergoes a significant reduction in pitch amplitude already for modest stiffnesses, this is observed since the central platform is the most sheltered one, this being constrained on both sides. Finally regarding the third platform, an increase in the amplitude of oscillation is observed for low values of connection stiffness, this is due to the fact that by applying the connection the third platform begins to be affected by the action of the others that precede it, but since the connection is very yielding this is not able to attenuate the oscillation. It is also observed that for high stiffness values it's influence on the motion of the platforms is greatly reduced, which means that the behaviour of the platforms for high stiffnesses is similar to that of a rigid body.

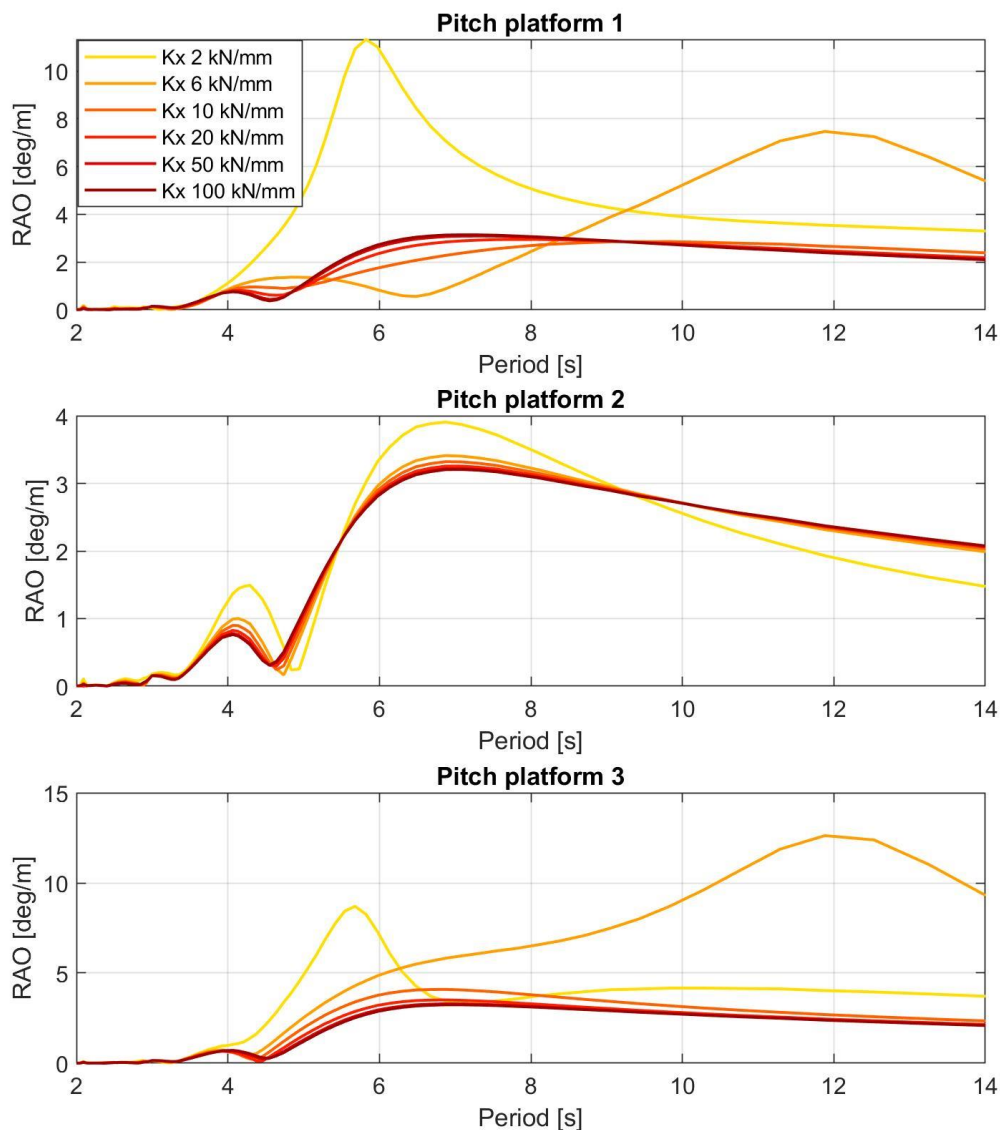


*Figure 4.12 RAO – max pitch platform 1 for variable  $K_x$  and  $K_z = 0.5 K_x$*

The increase in axial and lateral stiffness allows a significant reduction in elastomer shortening between platforms in both axial and lateral directions for all wave periods (Figure 4.13). In particular, it is observed that for stiffnesses  $K_x$  of less than 10 kN/mm and  $K_z$  of 5 kN/mm the attenuation is reduced, and resonance is observed shifting to larger periods as stiffness increases. For greater stiffnesses, resonance is not observed; a maximum is observed at periods of about 7s, the magnitude of which decreases as stiffness increases, assuming the behaviour of a rigid body.

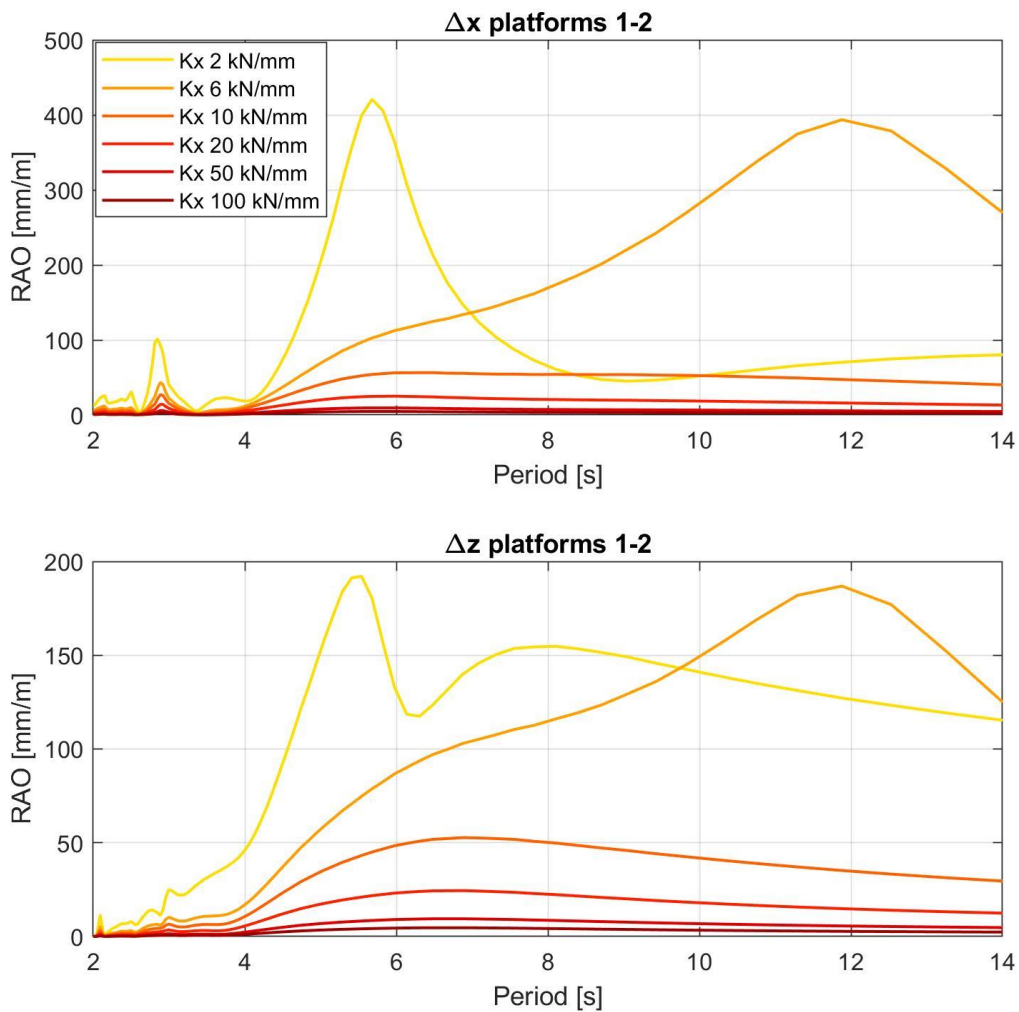


**Figure 4.13** RAO – max deformations between platforms 1-2 for variable  $K_x$  and  $K_z = 0.5 K_x$

The forces exchanged between the platforms have a similar trend to that of the shortenings, with a maximum that for modest stiffnesses moves toward greater periods as stiffness increases (Figure 4.14). For stiffnesses greater than 10 kN/mm the magnitude of the forces exchanged varies little with the stiffness of the connection, since an increase in stiffnesses corresponds to a corresponding reduction in shortenings. It is found that at an increase in stiffness, for the same wave period, the forces exchanged are reduced; the effect of reducing the shortening between platforms therefore has a greater impact than increasing stiffnesses.

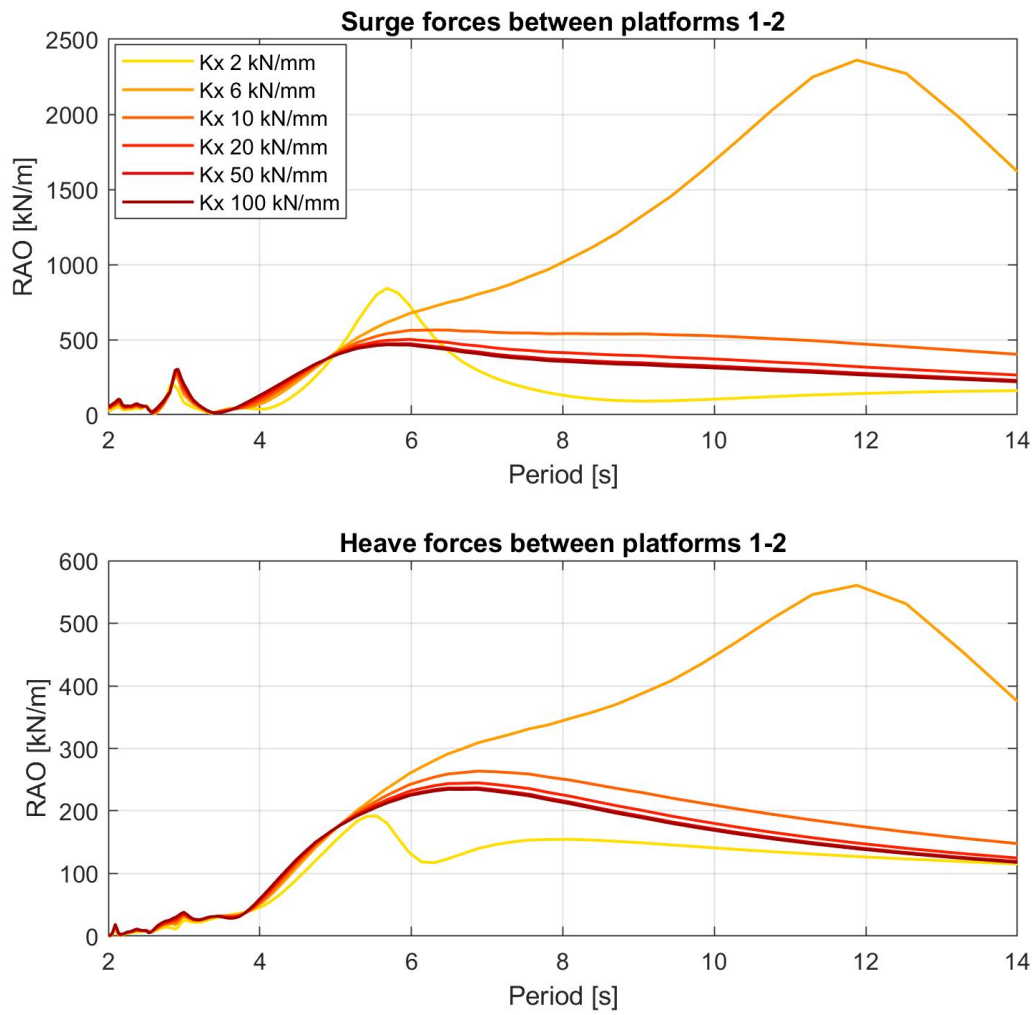


**Figure 4.14** RAO – max forces between platforms 1-2 for variable  $K_x$  and  $K_z = 0.5 K_x$

### 4.3 Irregular wave analysis

The natural seaway on the oceans is irregular. It is also referred to as random sea, or as confused sea. The sea shows rarely a unidirectional, regular sinusoidal wave pattern, but we observe a mixture of waves of different length, height, and direction.

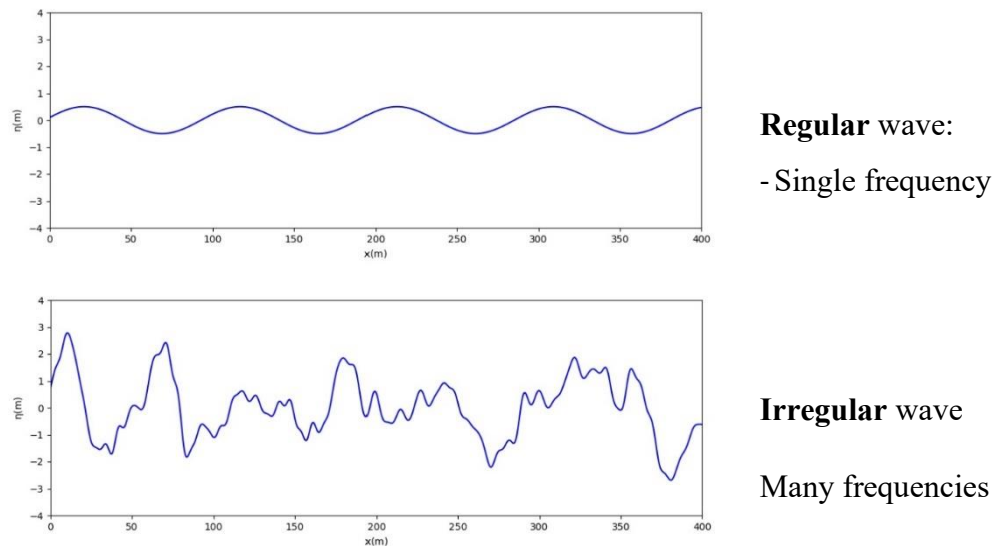


**Figure 4.15** Regular and irregular wave

The natural seaway can be decomposed to a sum of partial sinusoidal waves, each having a relatively small steepness, even for a severe sea. Therefore, the spectral approach with a sum of partial waves constitutes a valid representation for a random sea. From careful observation, certain typical or characteristic parameters can be estimated [23].

Dimensions	Description	Value
$H_{max}$	Largest wave height in the sample	$H_{max} = \max_i(H_i)$
$H_{av}$	Mean wave height	$H_v = \frac{1}{N} \sum H_i$
$H_{rms}$	Root-mean-square wave height	$H_{rms} = \sqrt{\frac{1}{N} \sum H_i^2}$
$H_{1/3}$	Average of the highest $N/3$ waves	$H_{1/3} = \frac{1}{\frac{N}{3}} \sum_1^{\frac{N}{3}} H_i$
$H_{m0}$	Estimate based on the rms surface elevation	$H_{m0} = 4 (\eta^2)^{\frac{1}{2}}$
$H_S$	Significant wave height	Either $H_{1/3}$ or $H_{m0}$

**Table 4-2** wave's height characteristic parameters

Dimensions	Description
$T_S$	Significant wave period (average of highest $N/3$ waves)
$T_P$	Peak period (from peak frequency of energy spectrum)
$T_e$	Energy period (period of a regular wave with same significant wave height and power density; used in wave-energy prediction; derived from energy spectrum)
$T_z$	Mean zero up-crossing period

**Table 4-3** wave's period characteristic parameters

For a narrow-banded frequency spectrum the probability distribution of wave heights the Rayleigh probability distribution is appropriate. The probability density functions is:

$$f(H) = 2 \frac{H}{H_{rms}^2} e^{-\left(\frac{H}{H_{rms}}\right)^2}$$

The spectrum provides the information about the distribution of the wave energy among the different wave frequencies (or wave periods) or wavelength on the sea surface being analysed. The spectral density can be defined as an image that identifies the relative wave energy presenting all frequencies or periods at a fixed location or region for a predefined time period, regardless of the energy's directional heading. In other words, it shows at which frequencies variations are strong and at which frequencies variations are relatively weak.

We're interested in the power spectrum of the waves, the energy in a wave is proportional to  $\eta^2$ , where  $\eta$  is surface displacement while the energy spectrum, or power spectrum, is the Fourier transform of  $\eta^2$ .

In order to define the distribution of energy with frequency we use the JONSWAP (Joint North Sea Wave Project) spectra, the underlying equation is:

$$S(\omega) = \frac{\alpha g^2}{\omega^5} e^{-[\beta \frac{\omega_p^4}{\omega^4}] \gamma^a}$$

Where,

$$a = \exp \left[ -\frac{(\omega - \omega_p)^2}{2 \omega_p^2 \sigma^2} \right]$$

$$\sigma = \begin{cases} 0.07 & \text{if } \omega < \omega_p \\ 0.09 & \text{if } \omega > \omega_p \end{cases}$$

$$\beta = \frac{5}{4}$$

$\alpha$  is a constant that relates to the wind speed and fetch length.

$\omega$  is the wave frequency

$\omega_p$  is the peak wave-frequency

The irregular wave analysis allows us to simulate real sea states, based on which the effect of different combinations of axial and lateral stiffness on the motion of the platforms are evaluated. Three different sea states were simulated, with height  $H_s = 0.5\text{m}$  and periods of  $T_p = 2\text{s}$ ,  $T_p = 4\text{s}$ , and  $T_p = 6\text{s}$ .

The study of maps in irregular wave allows us to clearly distinguish the effect of individual axial and lateral stiffnesses (Figure 4.16). The greatest effect on platform pitching is given by the value of axial stiffness, the effect of lateral stiffness is greatly reduced. As the wave period increases there is an increase in the pitch of the platforms for each combination of stiffnesses, this is due to the fact that for longer period waves there is also greater wavelength, and when this becomes similar to the size of the connected platform system this goes into resonance amplifying the pitching. For periods of 2 and 4 seconds as axial stiffness increases there is a decrease in platform pitching; in fact, resonant wave periods stress the platforms taken individually much more than when connected, and the addition of a connection makes them less susceptible to these wave periods. For longer wave periods, e.g.,  $T = 6\text{s}$ , for reduced stiffnesses the pitching of the platforms is reduced because waves of longer wavelengths stress much less the platforms taken individually. As stiffness increases, the system behaves more and more like a rigid body, and for this reason it is more stressed by longer wavelength waves, this results, as detectable from the third graph, in increased pitching as the stiffness of the connection increases.

This finding strongly supports the choice of using elastomeric bearings for the design of the connection, since these have a much higher axial stiffness that is easily modified by changing the construction parameters, compared to the lateral stiffness, which it has been noted how it changes relatively little by modifying the geometry of the bearings.

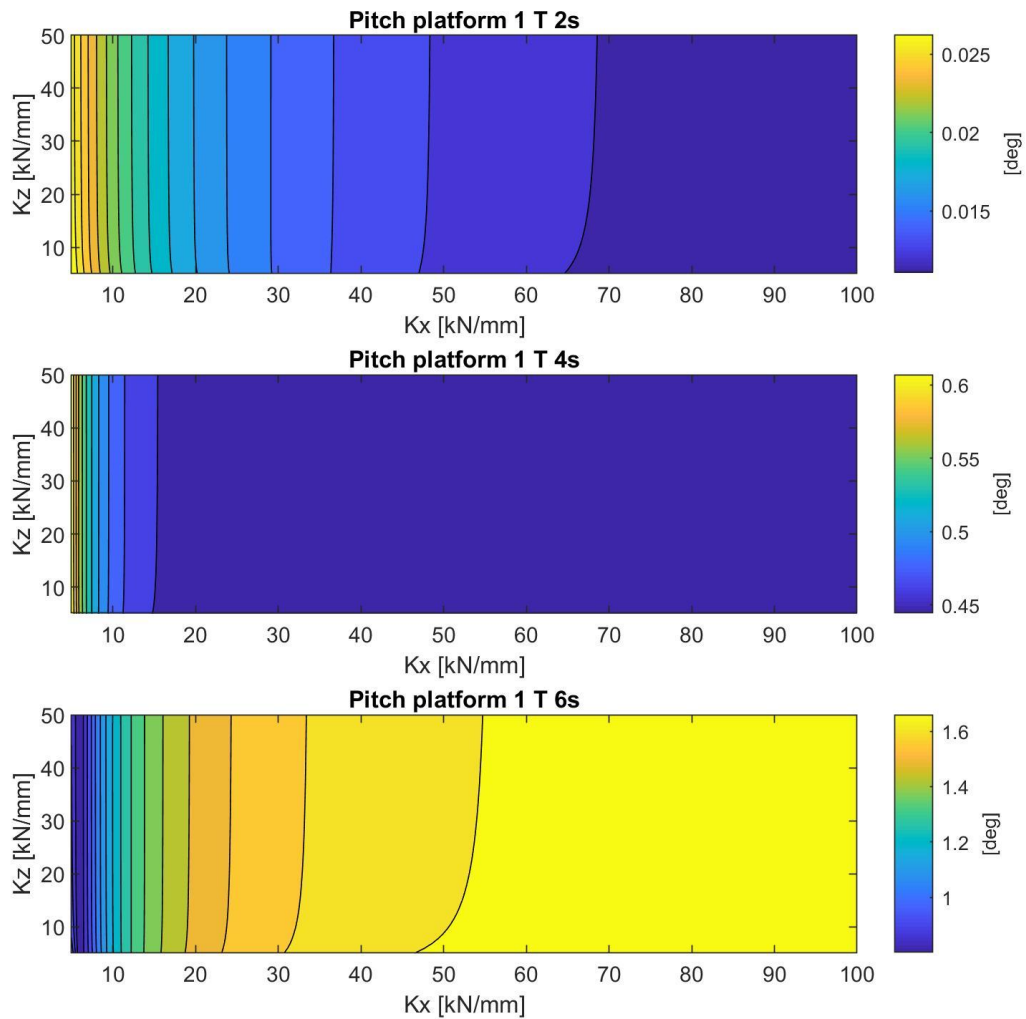


**Figure 4.16** Maps –max. pitch platform 1 for  $T = 2-4-6 s$

The greatest effect on the axial deformation of the connection is given by the value of axial stiffness (Figure 4.17); the effect of lateral stiffness is greatly reduced. As the wave period increases, there is an increase in the deformation of the connection for any combination of stiffnesses. The small axial stiffness generates considerable deformations already for wave periods of 4 s, as stiffness increases this value rapidly decreases up to stiffnesses of 50 kN/mm and then continues to decrease but more slowly for larger axial stiffnesses.

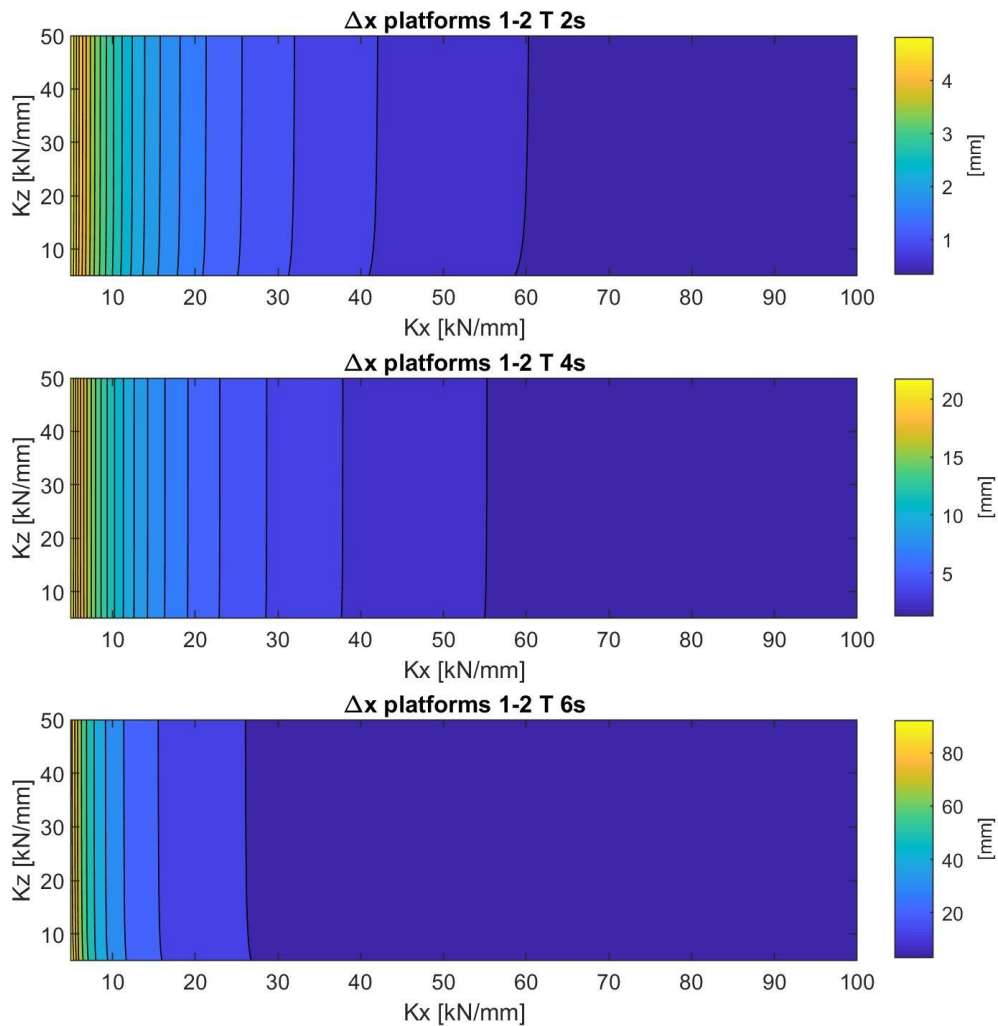


**Figure 4.17** Maps – max. axial deformations between platforms 1-2 for  $T = 2-4-6 s$

The greatest effect on the lateral deformation of the connection is given by the value of lateral stiffness (Figure 4.18); the effect of axial stiffness is greatly reduced. As the wave period increases, there is an increase in the deformation of the connection for each combination of stiffnesses. The magnitude of lateral deformations is significantly less than those in the axial direction, for each combination of stiffnesses and for each wave period. This is due to the fact that the forces in the Heave direction are much smaller than those in the surge direction.

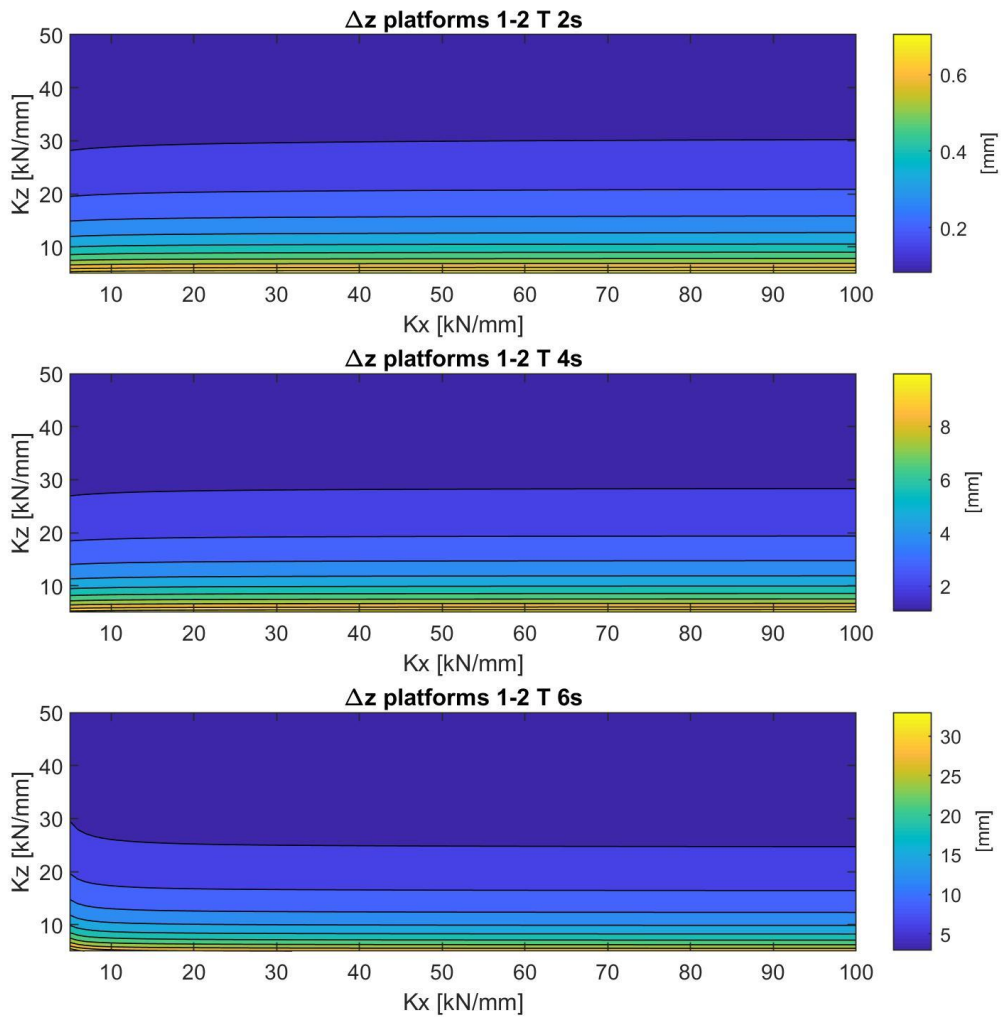


**Figure 4.18** Maps – max. lateral deformations between platforms 1-2 for  $T = 2-4-6$  s

The surge forces exchanged between the platforms (Figure 4.19) have an increasing trend for periods of 2 and 4 s, while they exhibit a maximum for lower stiffness values and then decrease as stiffness increases in the case of  $T = 6$ . The reasons for this are to be found in the trend of deformations in the x-direction, described earlier. For each value of axial stiffness, there are bigger exchanged forces for larger wave periods because of the larger deformations that occur under these conditions.

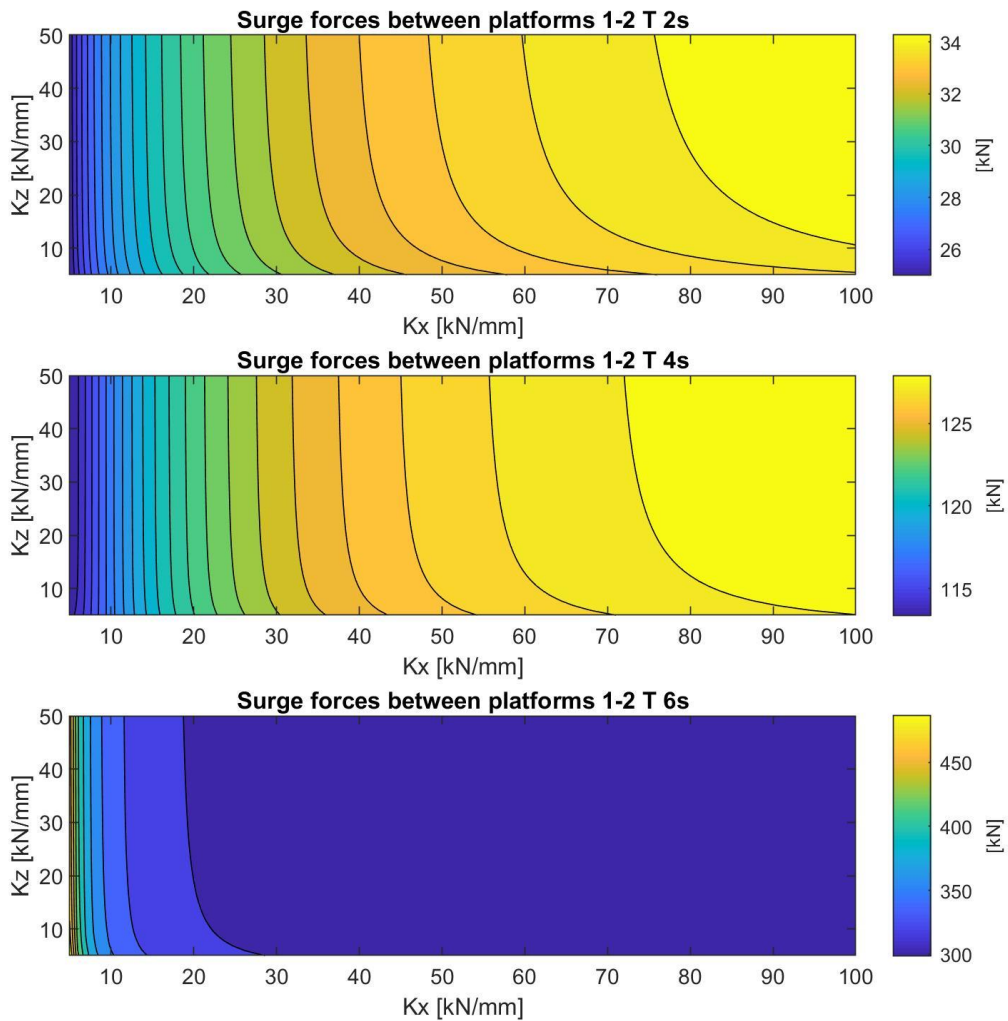


**Figure 4.19** Maps – max. surge forces between platforms 1-2 for  $T = 2-4-6$  s

The heave forces exchanged between the platforms (Figure 4.20) have an increasing trend for periods of 2 and 4 s, while they exhibit a maximum for lower stiffness values and then decrease as stiffness increases in the case of  $T = 6$ . The value of the exchanged forces is lower than the forces in the surge direction because of the lower strains; unlike the latter, moreover, a substantial effect of the lateral stiffness value on the exchanged forces is observed. For each value of axial stiffness, there are larger exchanged forces for larger wave periods, because of the larger deformations that occur under these conditions.

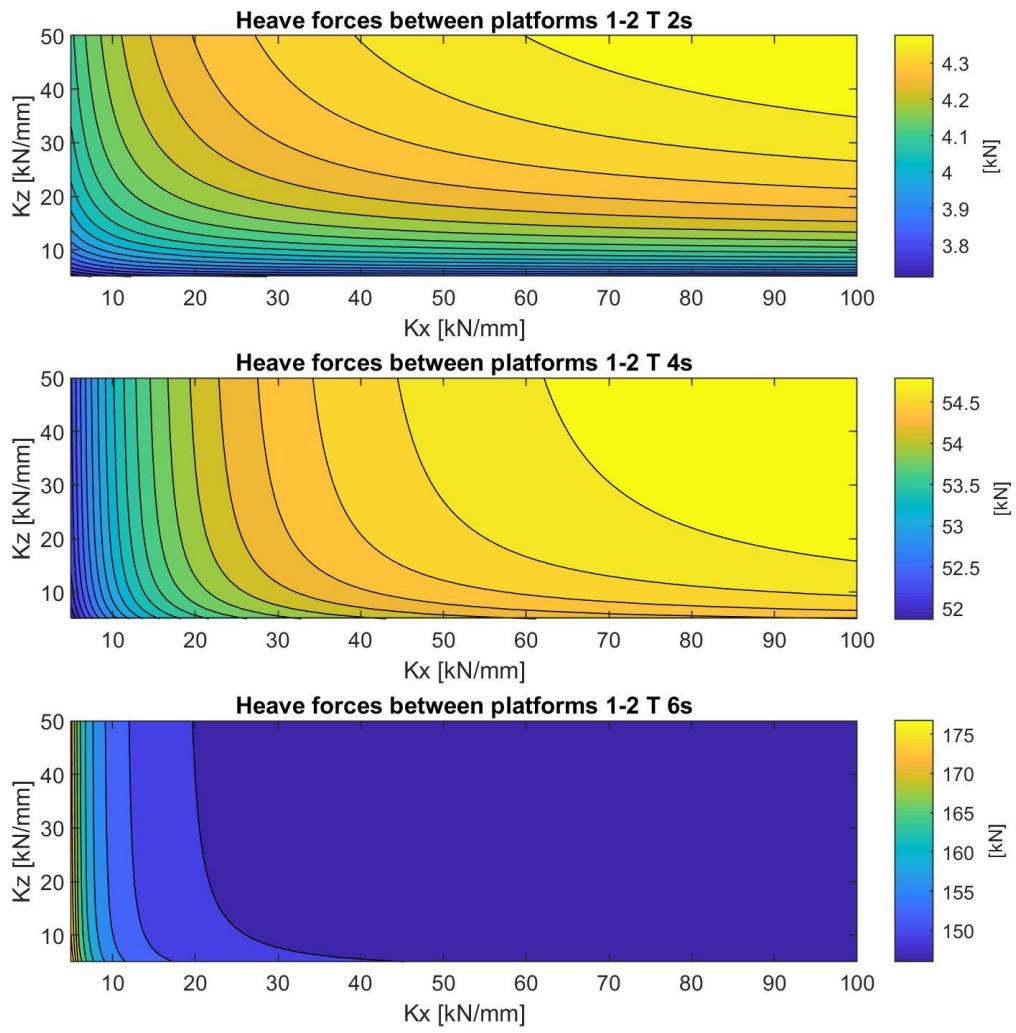


**Figure 4.20** Maps – max. heave forces between platforms 1-2 for  $T = 2-4-6$  s

#### 4.4 Comfort Criteria

In order to identify allowable rigidities for the system, it is necessary to identify what are the comfort limits within which it is necessary to be in order for the platforms to be used for living purposes. These limits were identified during the Living@Sea project [24], the vision of this project is to create a sustainable and safe city on water, considering the demands of the inhabitants and the environmental conditions.

<b>Limiting Criteria</b>	<b>Limiting value</b>
Inclination for floating residential areas	1 degree
Max vertical height difference between module edges	ideally only 10 mm max. RMS 0.15
Vertical accelerations/heave motion	m/s <sup>2</sup> max. RMS 0.03
Horizontal accelerations/lateral motions	g
Max metres of green water on deck	0 m

*Table 4-4 limiting comfort criteria*

By applying the above criteria to the maps obtained for irregular waves, it is possible to eliminate from the maps the combinations of axial and lateral stiffnesses that do not guarantee compliance with one or more of the criteria listed above.

Below are the maps obtained by eliminating the above stiffnesses from the map, the values shown in the maps are those of forces exchanged between the platforms, on them in fact no limit has been placed. A limit to the axial deformation will be placed during the sizing of the elastomeric bearings.

For period of 3 s almost all the stiffnesses obtainable from elastomeric bearings are permissible (Figure 4.21), this is because the motion of the platforms is small for these wave periods, and small stiffnesses are sufficient for the comfort limits to be met. The greatest values of exchanged forces occur along the axial direction, this is because the stiffnesses are

considerably greater along this axis. It is also observed that the magnitude of the exchanged forces increases as stiffness increases, although this leads to a reduction in the relative displacement to which the forces are proportional. There is also a decisive increase in the exchanged forces at stiffnesses compared to the sea state case with a period of 3s, this is evidently due to the increased relative displacement between the platforms.

For period equal to 4s the range of possible stiffnesses is reduced along both x and z, an increased sea state therefore requires the use of higher stiffnesses to limit the motion of the platforms and ensure comfort limits. The largest values of exchanged forces also occur in the axial direction, it is also observed that here too the magnitude of the exchanged forces increases with increasing stiffness, although this results in a reduction in the relative displacement to which the forces are proportional.

For period of 5 s the range of possible stiffnesses is reduced more, the largest values of exchanged forces also occur in the axial direction, but a substantial difference is observed: the magnitude of the exchanged forces decreases as the stiffness increases. This is due to the fact that for wave periods between 5-6 s the system goes into resonance, as the wavelength becomes comparable to the length of the platform system. For small stiffnesses, the motion of the platforms is so accentuated by resonance that the forces exchanged reach a maximum value for these stiffnesses, due to the high relative displacements between the platforms. As stiffness increases, the relative displacements become smaller, leading to a reduction in the forces exchanged.

Observing how the maps showing the stiffness combinations that guarantee compliance with the comfort parameters change as the simulated wave period changes, we find that the range of permissible stiffnesses narrows considerably as the wave period increases, corresponding, as noted earlier, to very pronounced platform motions.

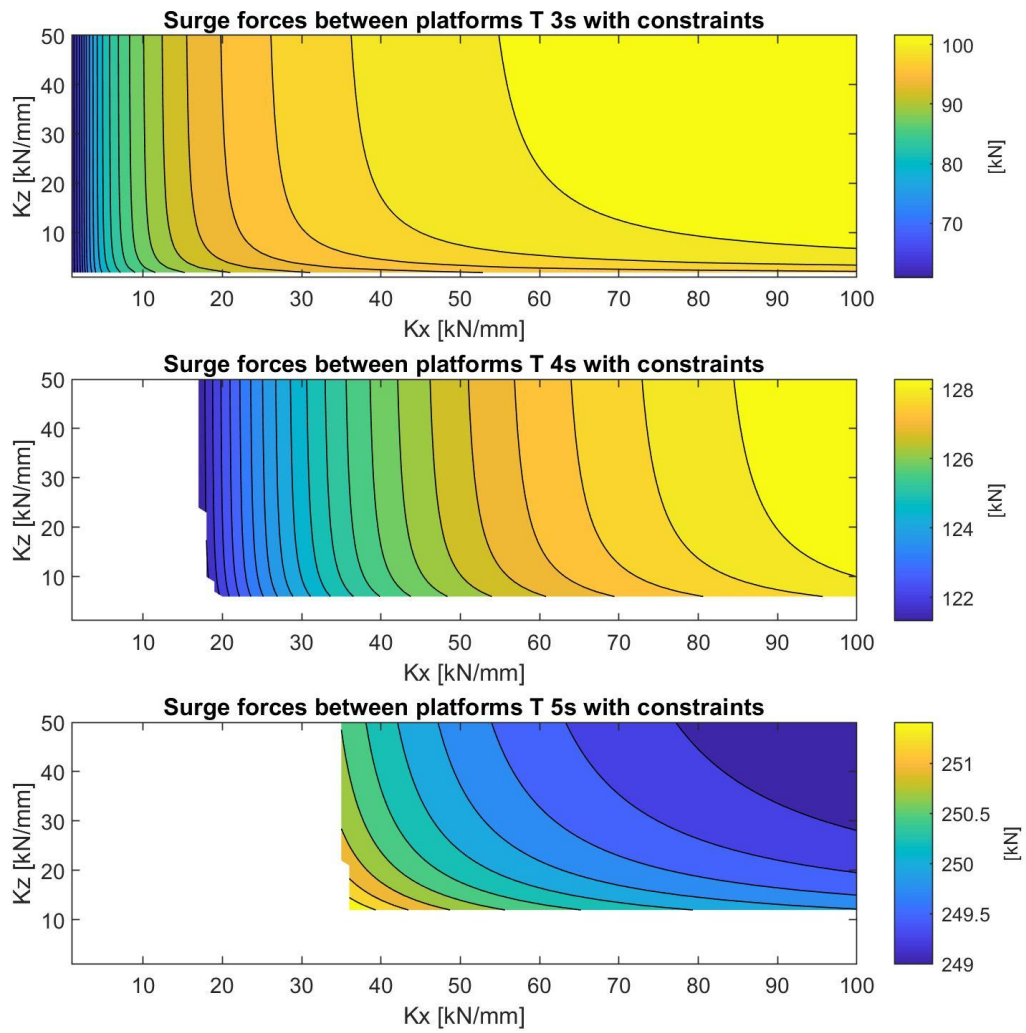


**Figure 4.21** Constrained maps – max. surge forces for  $T = 3-4- 5s$

## 5. Connection design

The design of the connection aims to position the elastomeric bearings in such a way that they can effectively be active when there is shortening or elongation of the distance between the platforms. This is a nontrivial result to achieve because by their nature elastomeric bearings work only in compression and not in tension, so it is necessary to design a system that allows the elastomeric bearings to go into compression when the distance between the platform increases.

After the identification of the right disposition of the bearings, the actual sizing of the elastomeric bearings is carried out, taking into account the results obtained from the irregular wave simulations, which made it possible to identify the minimum stiffness values that must be respected in order for the comfort parameters to be met.

### *5.1 Constructive solution*

The constructive solution hypothesized involves obtaining compartments within the platforms (Figure 5.1), in which to place the elastomeric bearings; these are placed in tension through the use of steel strands, such a configuration allows the relative receding motion of each platform to be transmitted to the other, inducing a compression of the bearings.

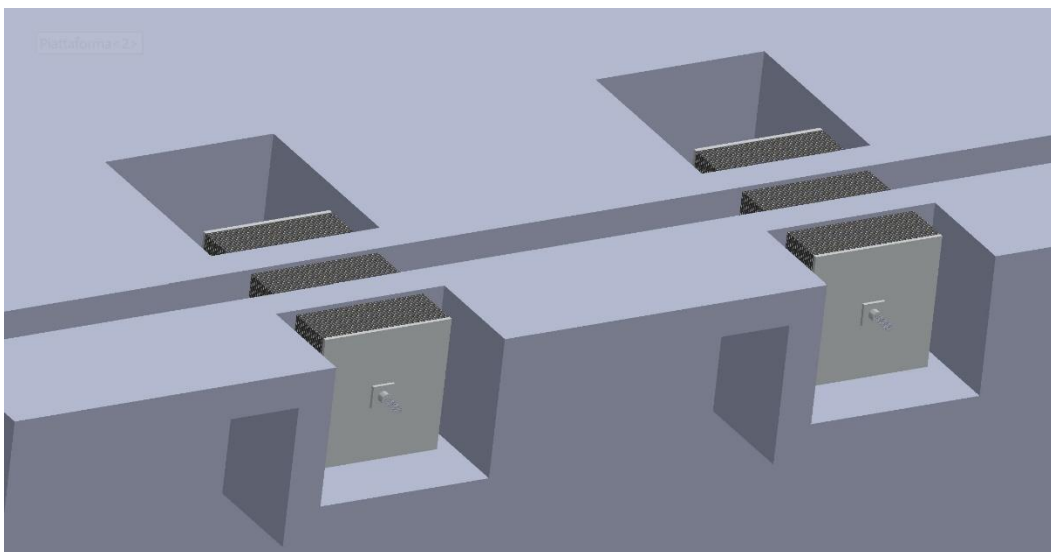


**Figure 5.1** detail of compartments and bearings

For relative approach motion, on the other hand, the bearings positioned between the platforms, in parallel with each other, are the ones that oppose resistance to the motion (Figure 5.2). It should be noted that for such an arrangement the only bearings to resist lateral motion between the platforms are those positioned between the platforms, the strands by which motion transmission occurs for the bearings in traction are in fact incapable to transmit the lateral motion of the platforms.

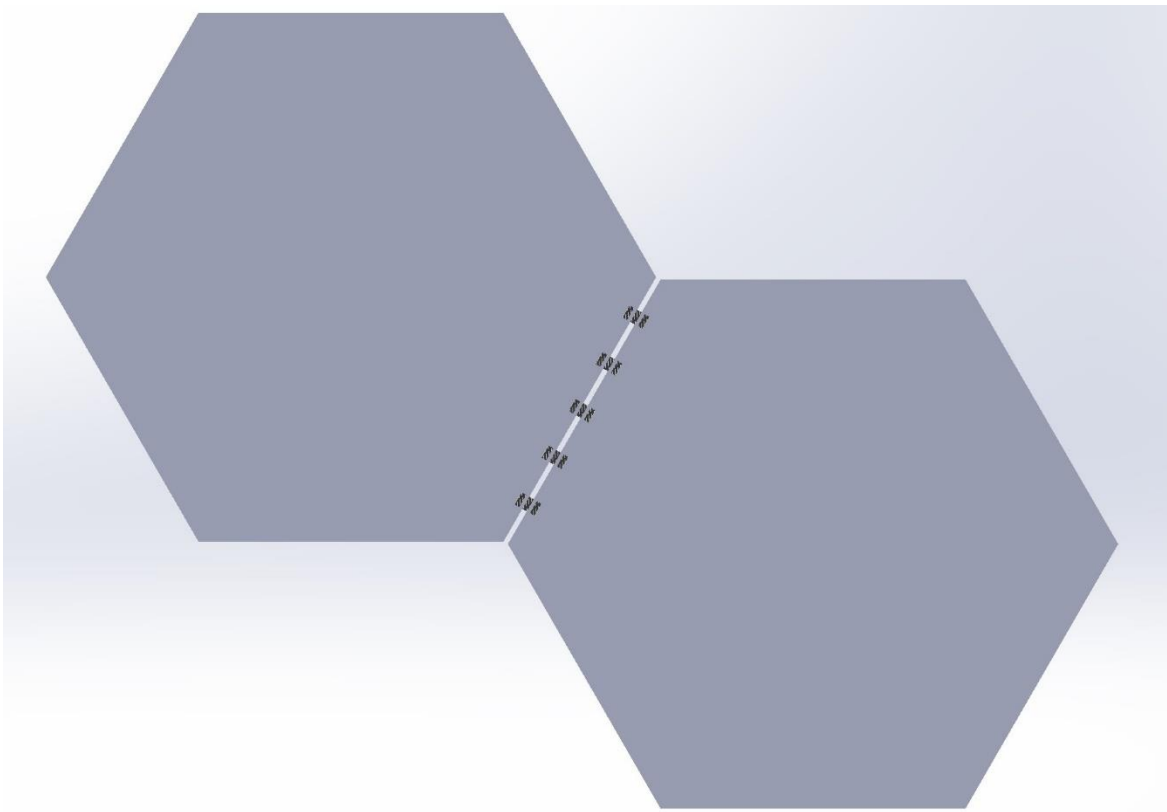


*Figure 5.2 view of the connection from above*

Finally, about the pitching of the platforms, depending on the direction of pitching motion, one row of bearings will be put in compression and the other one in tension, which is why it has been chosen a disposition of two rows of bearings between the platforms (Figure 5.3). Furthermore, both compression and tension bearings are placed at the same elevation, so as not to have inhomogeneity in torsional stiffness.

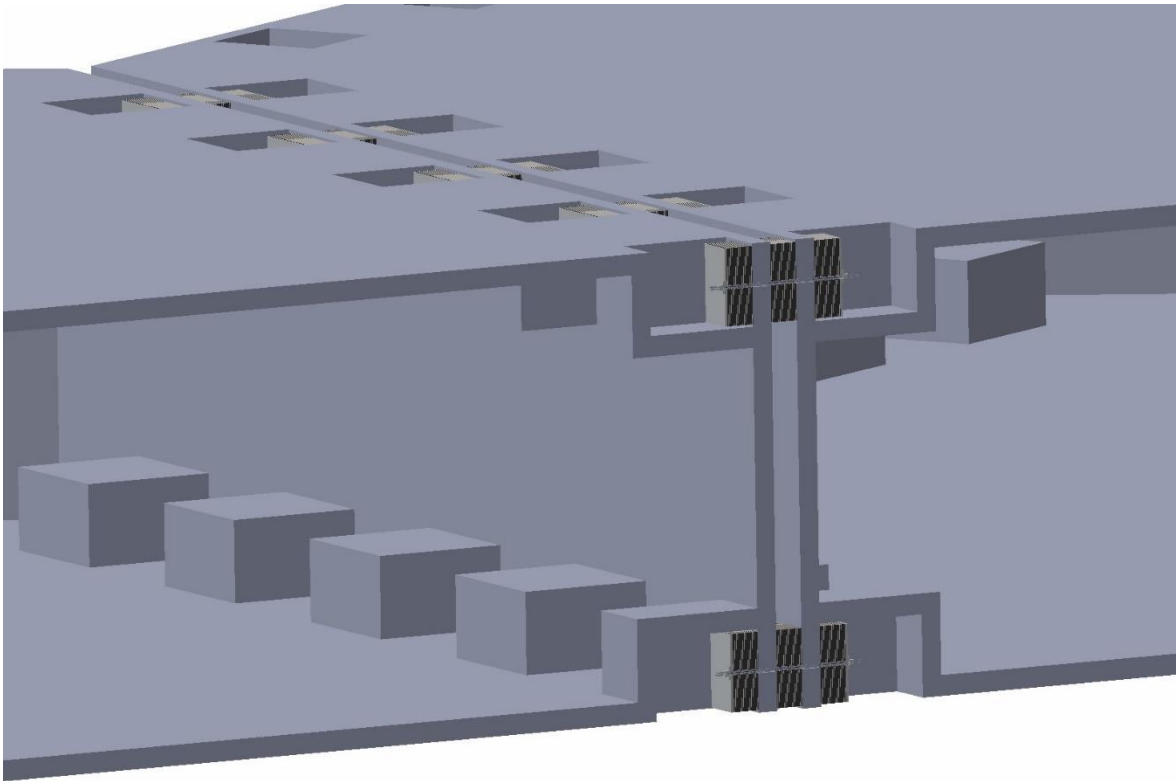


*Figure 5.3 detail fo the bearings traction system*

### *5.2 Equivalent stiffness*

Since the quantities of interest for this work are surge, heave, and pitch, the equivalent stiffnesses were calculated along the x and z axes, and the rotation around the y axis.

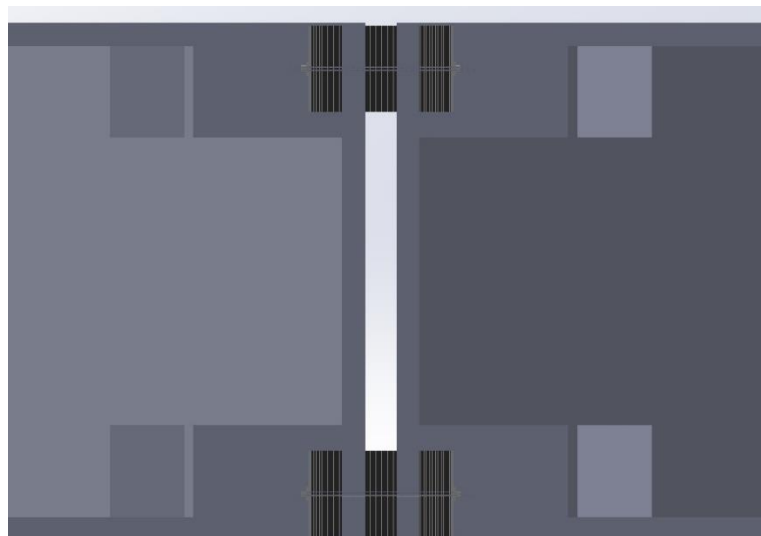


*Figure 5.4 side view of the connection*

Along the surge direction the bearings positioned between the two platforms result in compression as the relative distance between them decreases; since in presence of only the motion along x these bearings see the same shortening between them, they appear to be in parallel (Figure 5.4). Called  $K_c$  the axial stiffness of the single bearing and called  $n$  the number of bearings placed in compression; the equivalent compressive stiffness will be given by:

$$Kx_c = \sum_1^n K_c \quad (5.1)$$

Unlike the latter, the bearings placed in the compartments are shortened when the relative distance between the platforms increases. As they are arranged, in presence of only motion along x axis, these bearings appear to be placed in series with each other, thus the overall stiffness is reduced. Called  $K_t$  the axial stiffness of the single bearing and being two the number of bearings placed in traction for each couple of traction bearings; the equivalent tensile stiffness, will be given by:

$$\frac{1}{Kt'_x} = \sum_1^2 \frac{1}{K_c}$$

Considering a couple of bearings in traction we can write that:

$$Kt'_x = \frac{K_c}{2} \quad (5.2)$$

As for each pair of bearings in tension we have a bearing in compression ( $m = 2n$ ), we can write that,

$$Kx_c = Kx_t = Kx = \sum_1^n K_c \quad (5.3)$$

It is therefore found that the stiffness along x axis is equal in case of both compression or traction.

A similar study can be made for the calculation of equivalent lateral stiffness, paying attention to the fact that the only bearings which oppose effective resistance to the motion

along z are the ones placed between the two platforms. Between the bearings in traction, in fact, the forces are transmitted via pre-tensioned steel cables, which can transmit forces only along the x axis. Therefore, given  $K_t$  the lateral stiffness of the single bearing, we find that the lateral stiffness  $K_z$  is:

$$K_z = \sum_1^n K_t \quad (5.4)$$

Finally, we evaluate the pitching stiffness, in the presence of pitching we have that one row of elastomers is put in compression and one in tension, having called  $\Delta_x$  the shortening of the elastomers as a result of the pitching motion, we will have that the elastic forces opposing the motion are:

$$F_x = r K_c \Delta_x$$

Calling "a" the distance between the centre of the connection and the point of application of the elastomers, we can approximate the shortening  $\Delta_x$  as  $a * \theta$  where  $\theta$  represents the pitching angle. The elastic resistant moment will therefore be:

$$M_\theta = r K_c a^2 \theta N_c$$

Hence the pitching stiffness:

$$K_\theta = r K_c a^2 N_c$$

But  $r K_c N_c$  is the equivalent stiffness  $K_x$  found above, we can therefore write that:

$$K_\theta = \sum_1^n K_c a^2 = K_x a^2 \quad (5.5)$$

### *5.3 Bearings Dimensioning*

From the analysis of the maps obtained from the irregular wave studies, the minimum lateral and axial stiffness values required for the system to meet comfort constraints were derived. In this section the objective is to size a connection based on the use of the elastomeric bearings noted in Chapter 2. When talking about connection sizing the choice of several

parameters is implied, which we saw in Chapter 2 how they greatly influence the stiffness of the connection. These parameters include:

Constructive parameters	Symbol
Number of bearings placed for each row	$N_c$
Size of elastomeric pads	$a$
Choice of using unreinforced or reinforced bearings, and in this case choice of the number of steel plates to be used	$N_s$
Overall height of elastomer	$H$

*Table 5-1 elastomeric bearing's main constructive parameters*

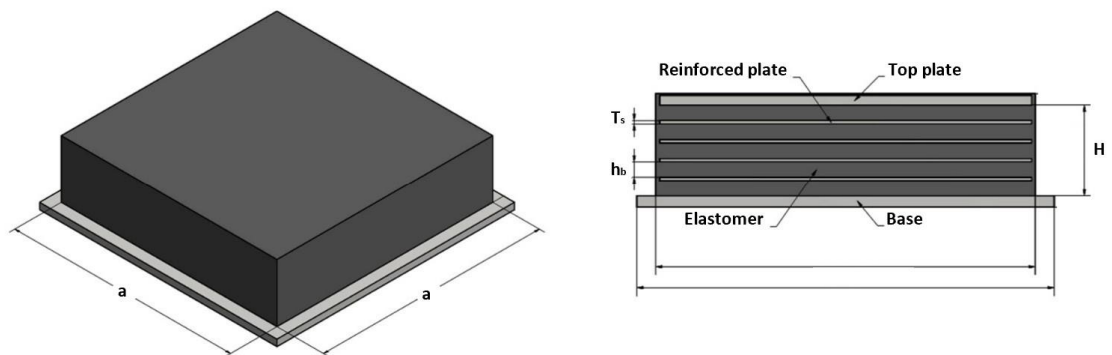


*Figure 5.5 elastomeric bearings main constructive parameters*

Instead, other parameters were set with the aim of making it easier to obtain the possible configurations; in particular, the number of rows of elastomeric bearings, equal to 2, the square shape of the bearings and finally the maximum lateral dimension of the pads, equal to 75 cm, were set.

Analyzing the axial and lateral stiffness ranges allowed by the elastomeric bearings and comparing them with the values found in the maps obtained from the irregular wave study, it is clearly observed that the limiting factor is the equivalent lateral stiffness. For example, it is observed that the addition of reinforcing steel layers does not have a major impact on the lateral stiffness if the total elastomeric thickness remains the same. This observation is

the basis for writing the algorithm that allows us to obtain the curves with the possible elastomer configurations.

In fact, the algorithm for a certain range of dimensions "a" which has been noted to be superiorly limited to 75 cm, calculates the axial stiffness for a set of decreasing values of H, in doing so it has been noted from the graphs obtained in Chapter 2, there is an increase in both axial and lateral stiffnesses. The algorithm stops when it finds the maximum value of H that provides the minimum desired lateral stiffness for a set of a, Nc, and Ns; stopping in correspondence of the minimum desired value of Kz the value of axial stiffness is minimized.

This allows us to generate curves in which for each value of "a" there is a value of H that guarantees the minimum lateral stiffness while minimizing the value of axial stiffness. This calculation is then repeated for different values of number of bearings per row Nc.

The only parameter that seems to be excluded from the algorithm for finding configurations appears to be the number of reinforcing steel plates, in fact this is a choice since it has been noted that the addition of steel plates results in a substantial increase in axial stiffness without a corresponding increase in lateral stiffness, so there is no doubt that the number of steel plates to be used is the minimum possible, and the idea of using unreinforced bearings has also been considered.

However, the absence of steel plates may lead to a problem with the stability of the bearings, in fact the bearing may become thick enough that instability affects their performance and bearing that is too tall and slender will fail by buckling, so stability is a potential problem, although only for relatively thick bearings. To assess whether conditions exist for using unreinforced bearings, the value of the parameter "a/H" was reported for the different possible configurations that guarantee the minimum lateral stiffness derived from the maps, which is 20 kN/mm, while minimizing axial stiffness.

In the case of reinforced bearings (Figure 5.6 ), the parameter  $H_{eff}$  refers to the sum of the thickness of the elastomer layers. It can be noted from the graphs that the a/H parameter varies very little for configurations with reinforced and unreinforced bearings. However, the stability limits in the two cases are different: taking the AASHTO Specifications [25] as a reference, the stability of the bearings is ensured by the limitation of the effective thickness of rubber, particularly for reinforced bearings the stability is ensured by the condition:

$$\frac{a}{H} > 3$$

While for unreinforced bearings, stability is ensured by the condition:

$$\frac{a}{H} > 5$$

Looking at the graphs of possible configurations for unreinforced bearings, it is observed that there are no stable configurations, i.e., with  $\frac{a}{H} > 5$ . So, although the configurations with unreinforced bearings offers lower axial stiffness, we are forced to choose a reinforced configuration for stability issues. It can be noted that among the possible configurations with reinforced bearings there are several curves above the limit value of  $\frac{a}{H_{eff}} > 3$ .

At this point the number of steel plates to insert is studied, for this purpose the axial stiffness value for configurations with bearings reinforced with 1 or 2 steel plates is reported. Only the curves for which the stability limit noted above is met are specifically reported.

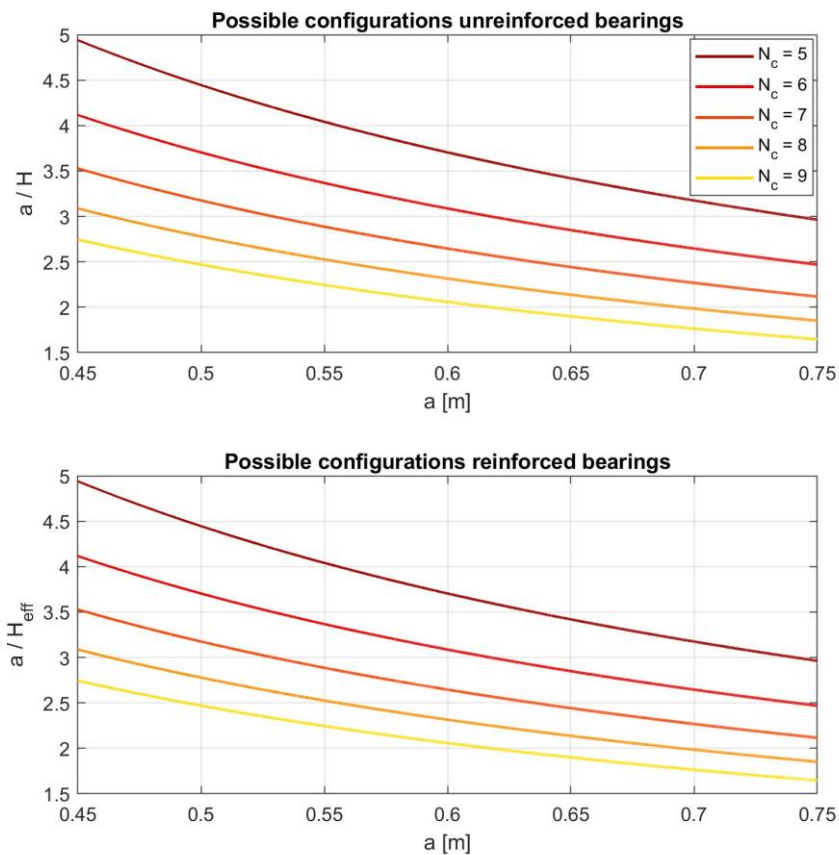


**Figure 5.6** possible bearings configurations –  $a/H$  stability parameter for different values of  $a$  and  $N_c$

From Figure 5.7 it can be observed that in order to minimize axial stiffnesses, it is appropriate to choose a configuration with only one reinforcing steel plate; such a configuration, in fact, allows us to comply with the stability constraint while having a fair number of configurations to choose from. Finally, note how the application of the constraint on the ratio  $\frac{a}{H_{eff}}$  caused some configurations to be greatly reduced, until they disappeared, in particular the configurations with high number of bearings for example in the case of  $N_c = 9$ . In these configurations, in fact, the minimum value of axial stiffness was found by the algorithm for big total heights of the bearings. The high number of bearings is in fact compensated with limited axial stiffness of the individual elements due to the considerable overall height.

In order to determine the most advantageous configuration for our purposes, the curves obtained for stable configurations with bearings reinforced by a steel plate are reported.

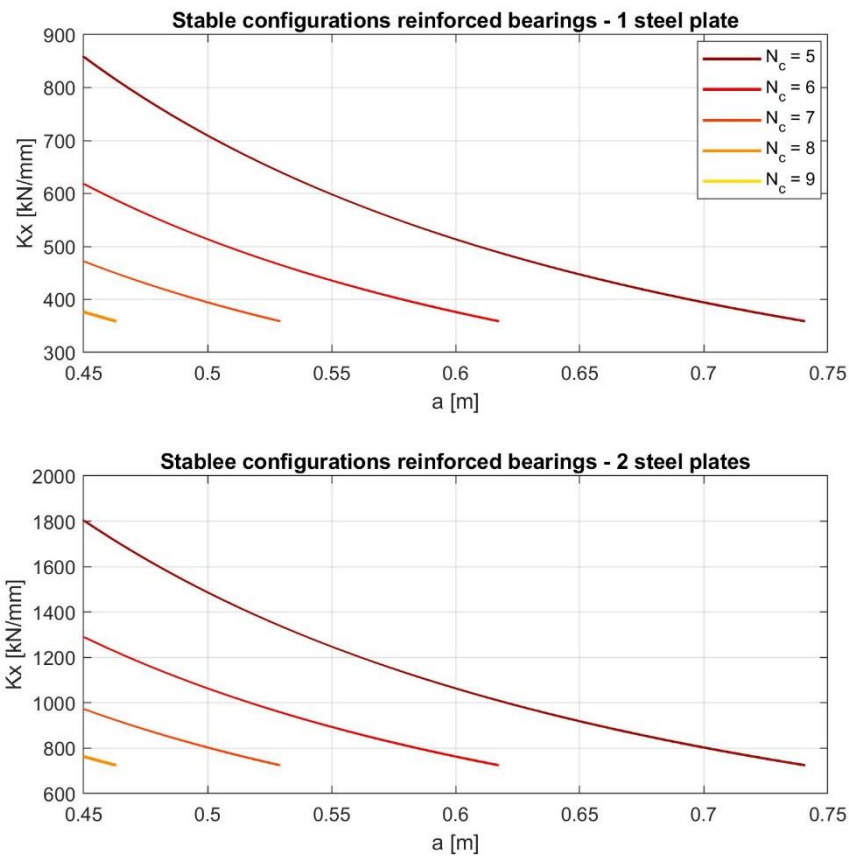


**Figure 5.7** stable bearings configurations – stiffness for different values of  $a$  and  $N_c$

Figure 5.8 shows that for the same  $N_c$ , the most favourable conditions in terms of limiting axial stiffness occur for larger values of "a," compensated by larger overall heights of the bearings. The choice among the possible stable configurations at this point should be made following what are the design constraints posed, with a limitation on the minimum distance between the platforms a configuration with smaller  $N_c$  might be adopted, while with limits on the size of the elastomers a solution with larger  $N_c$  in order to guarantee the minimum lateral stiffness while minimizing the value of  $K_x$  might be adopted.

In our case, an intermediate configuration between the two has been selected, characterized by:

- $a = 0.6$  m;
- $H = 0.2$  m;
- $N_s = 1$ ;
- $N_c = 6$ ;

This configuration allows us to obtain stiffnesses equal to:

- $K_z = 20$  kN/mm;
- $K_x = 370$  kN/mm;

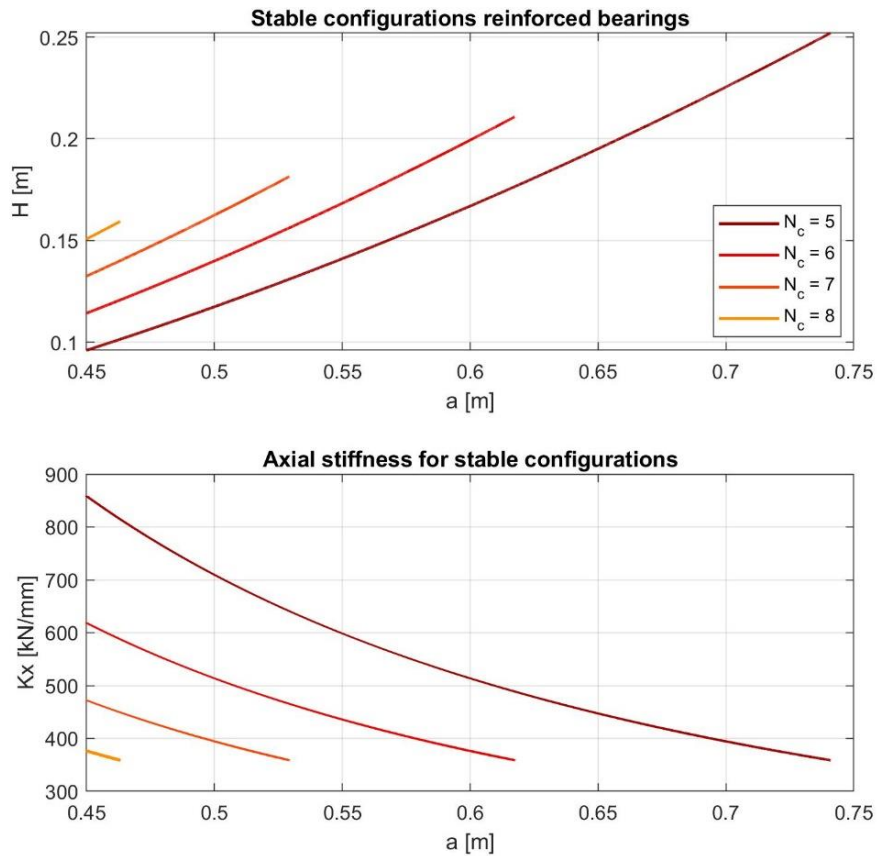


**Figure 5.8** stable bearings configurations –  $H$  and  $K_x$  for different values of  $a$  and  $N_c$

The maximum axial deformation is about 0.8 mm, and meets the stability criterion of the AASHTO Specifications: the maximum axial deformation should be less than 7% of the maximum bearing height, which is about 14 mm.

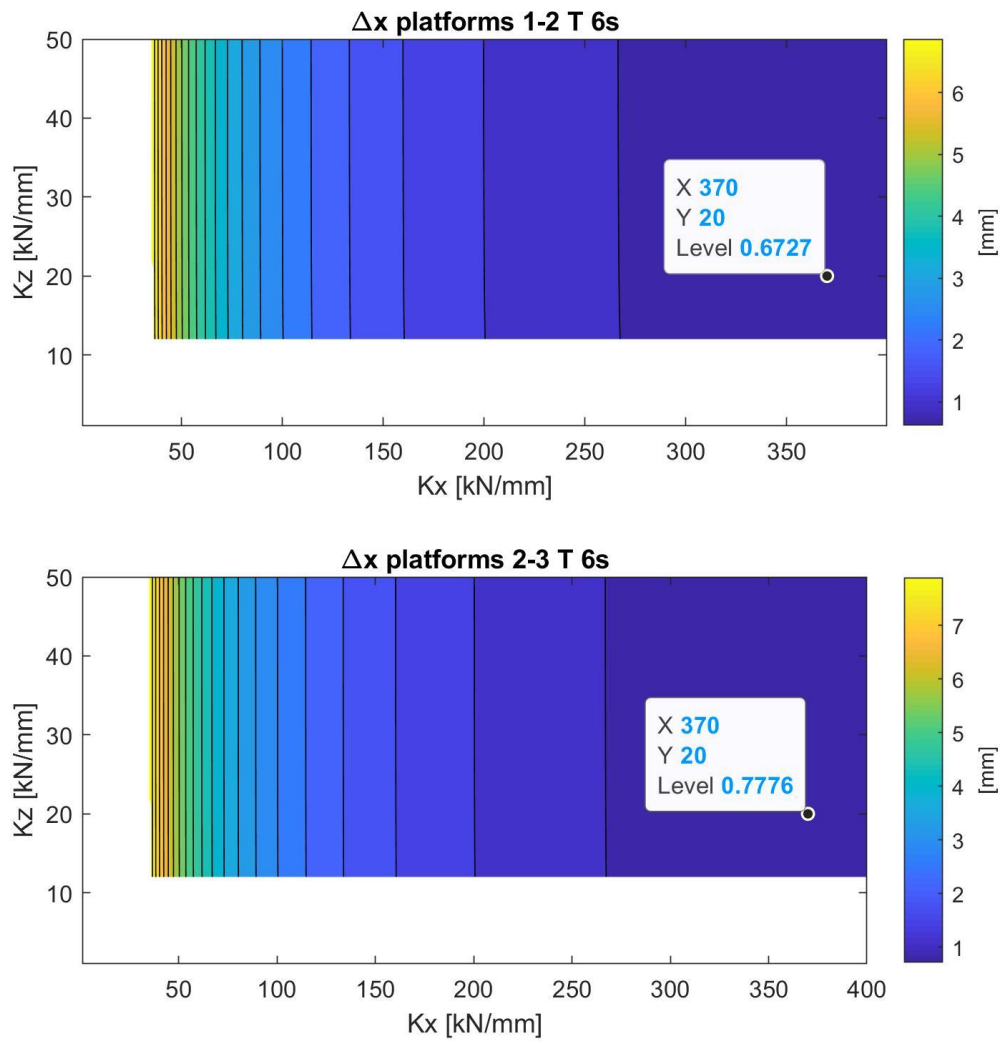


**Figure 5.9** Maps – max. axial deformations of bearings for  $T = 6s$

## Conclusions and future developments

In this work, an innovative elastic connection has been studied that would allow the connection of modular floating platforms, with the aim of improving the hydrodynamic response of the system. Numerical modelling of the connection, based on multibody system analysis, made it possible to derive a linearized stiffness matrix in the case of three platforms connected in series, which allows describing the behaviour of the platforms in the surge, heave, and pitch degrees of freedom.

The dynamics of the system were then studied through regular and irregular wave simulations as the stiffnesses of the connection changed, with the aim of optimizing its value, based on the comfort parameters the system must meet. In light of the stiffnesses required by the connection to guarantee the comfort parameters, the technology identified for the design of the connection is that of elastomeric bearings: a technology widely used in the civil sector that consists of an elastomer with a variable number of reinforcing plates, used to absorb high-frequency vibrations during earthquakes, which for this project was thought to be repurposed because of their stiffness characteristics, compatible with those required by the connection to effectively attenuate wave-induced platform motion.

Finally, the connection design was carried out, which consisted of finding the arrangement of elastomeric bearings capable of providing the required stiffnesses in both compression and traction directions. Finally, sizing of the connection took place by evaluating the geometric characteristics to be assigned to the individual bearings and their arrangement in terms of number of bearings to be installed.

The results obtained were satisfactory in the different works conducted: numerical modelling of the connection by the technique of multibody system analysis allowed obtaining a nonlinear model of the connection, which has been linearized in this work to facilitate computation during simulations of the system. The regular wave simulations made it possible to clearly distinguish the behaviour of the system as the wave period varies and for different values of stiffness, it has been noted that the system consisting of three platforms requires axial stiffnesses in the order of 10 kN/mm in order for the motion of the platforms to begin to feel the benefits offered by the connection, in terms of limiting pitching motions and reducing transmitted forces. It has also been observed that as the stiffness of the connections increases, the resonance of the system shifts toward higher periods; this is an

important result indicative of the fact that the system behaves for high stiffnesses of the connection, as a rigid body of characteristic size equal to the sum of the lengths of the platforms, and therefore resonated by waves of higher period (and consequently length).

The irregular wave study, on the other hand, allowed the effect of individual axial and lateral stiffnesses to be studied in more detail; it was observed that axial stiffness has a much more significant influence on the dynamics of the system, while the influence of lateral stiffness seems to be limited to the relative tangential motion between platforms and the forces exchanged in this direction. On the basis of the irregular wave study, it was also possible to identify the combinations of axial and lateral stiffnesses capable of guaranteeing the comfort and liveability criteria of the platforms, it has been noted that these ranges of stiffnesses are strongly dependent on the wave period considered and that in general they undergo a considerable reduction when higher wave periods are considered. This observation suggests that the increase in the number of platforms connected to each other may cause this range of stiffnesses that can be used for connection to vary considerably, an indication that the stiffness optimization should be repeated depending on the number of platforms used.

Finally, the bearings were sized in order to design a connection that provides the minimum stiffness values to guarantee the comfort parameters, the minimum lateral and axial stiffness values, evaluated from the most restrictive allowable stiffness maps corresponding to wave periods of 5s, were identified as 20 kN/mm and 50 kN/mm, respectively. The identified connection configuration was also found to comply with the stability limits of elastomeric bearings.

The natural development of this work involves the addition of mooring to the physical system, a factor that is expected to further constrain the motion of the platforms by relaxing the identified connection stiffness limits, and the analysis of the nonlinear model of the connection in order to identify similarities and any discrepancies from the linear model studied in this work. Further developments also involve building a scaled prototype in order to validate the obtained numerical model and adding degrees of freedom to the physical system, expanding the model to consider the three-dimensional effects of the connections on the various sides of the hexagon in various configurations.

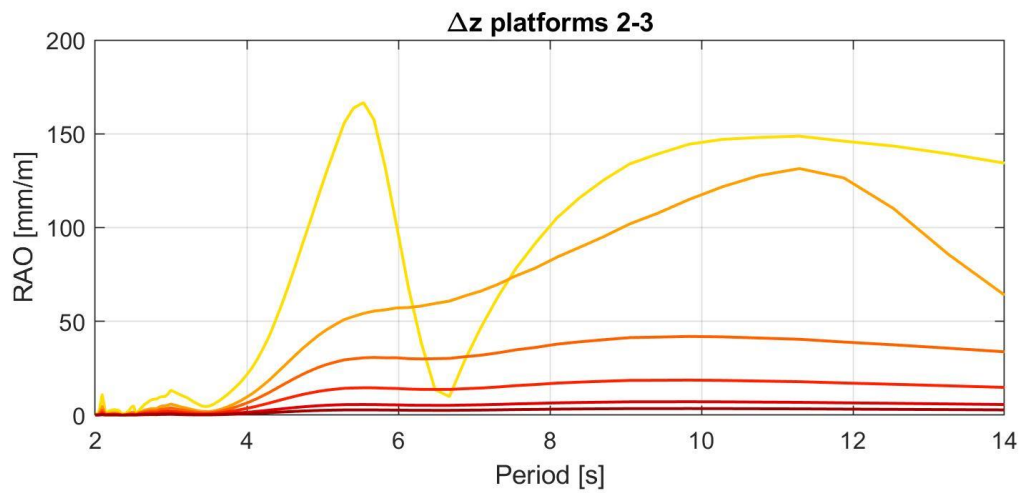
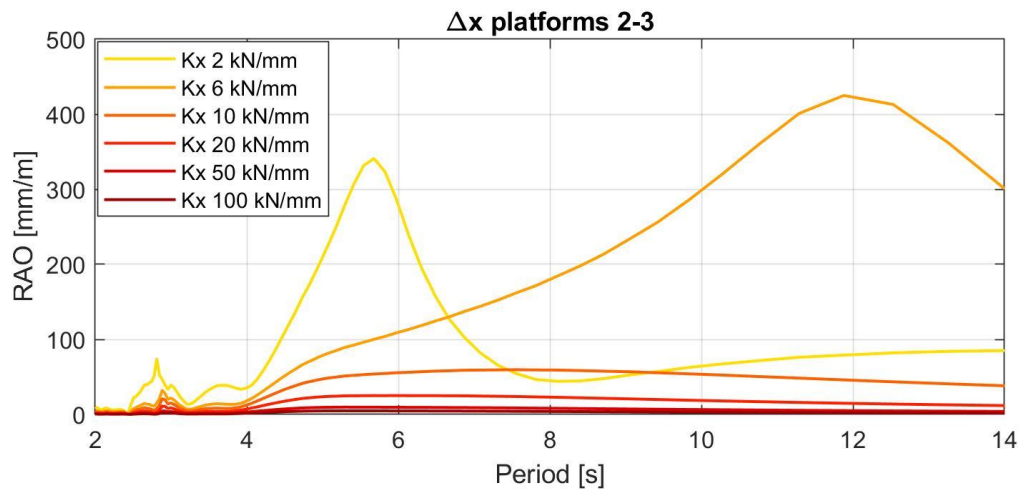
## Bibliography

- [1] James H. Diaz, in *Encyclopedia of Environmental Health (Second Edition)*, vol. 3, 2019
- [2] Alexey Andrianov, “Hydroelastic Analysis of Very Large Floating Structures,” Technische Universiteit Delft, 2005.
- [3] H. Tavana and M. J. Khanjani, “Reducing Hydroelastic Response of Very Large Floating Structure: A Literature Review,” *Int J Comput Appl*, vol. 71, no. 5, pp. 13–17, Jun. 2013, doi: 10.5120/12353-8658.
- [4] C. M. Wang, E. Watanabe, and T. Utsunomiya, *Very large floating structures*. CRC Press, 2006. doi: 10.1201/9781482265927.
- [5] D. Jiang, K. H. Tan, J. Dai, K. K. Ang, and H. P. Nguyen, “Behavior of concrete modular multi-purpose floating structures,” *Ocean Engineering*, vol. 229, p. 108971, Jun. 2021, doi: 10.1016/j.oceaneng.2021.108971.
- [6] C. M. Wang, M. Riyansyah, and Y. S. Choo, “Reducing Hydroelastic Response of Interconnected Floating Beams Using Semi-Rigid Connections,” in *Volume 4: Ocean Engineering; Ocean Renewable Energy; Ocean Space Utilization, Parts A and B*, Jan. 2009, pp. 1419–1425. doi: 10.1115/OMAE2009-79692.
- [7] R. P. Gao, C. M. Wang, and C. G. Koh, “Reducing hydroelastic response of pontoon-type very large floating structures using flexible connector and gill cells,” *Eng Struct*, vol. 52, pp. 372–383, Jul. 2013, doi: 10.1016/j.engstruct.2013.03.002.
- [8] D. Jiang, K. H. Tan, C. M. Wang, and J. Dai, “Research and development in connector systems for Very Large Floating Structures,” *Ocean Engineering*, vol. 232, p. 109150, Jul. 2021, doi: 10.1016/j.oceaneng.2021.109150.
- [9] H. Duan *et al.*, “Characterization and environmental impact analysis of sea land reclamation activities in China,” *Ocean Coast Manag*, vol. 130, pp. 128–137, Oct. 2016, doi: 10.1016/j.ocecoaman.2016.06.006.
- [10] Zhao, H., et al. *A flexible connector design for multi modular floating structures*. in *Proceedings of the ASME 2018 37th International*. 2018. Madrid, Spain.

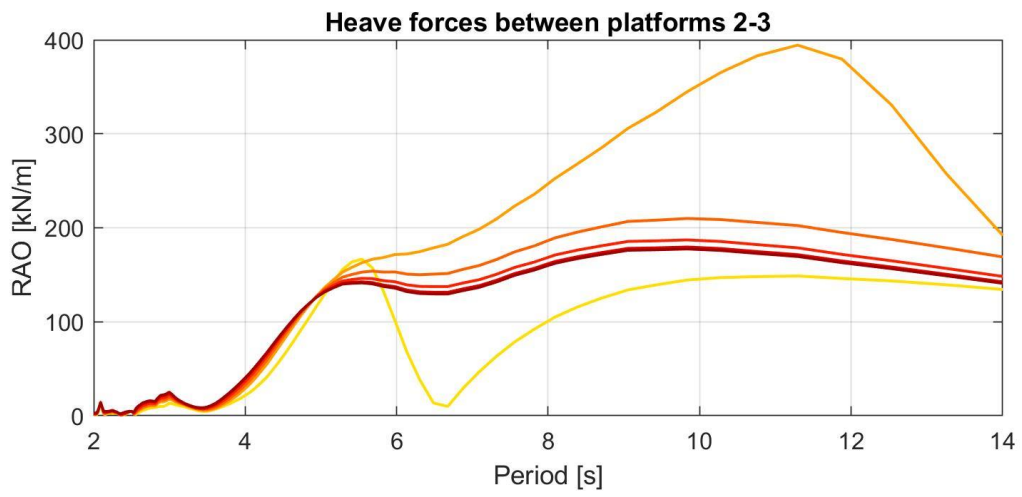
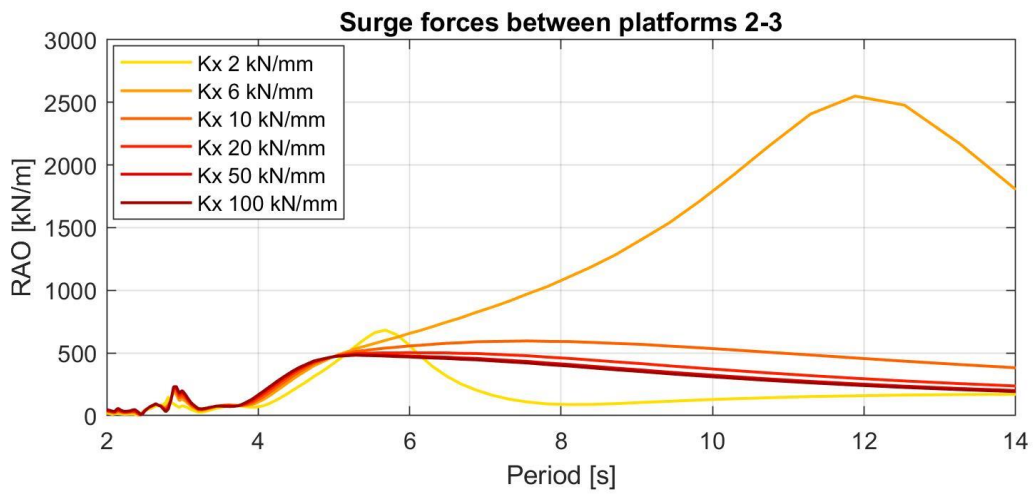
- [11] H. Zhao, D. Xu, H. Zhang, and Q. Shi, “A Flexible Connector Design for Multi-Modular Floating Structures,” in *Volume 1: Offshore Technology*, Jun. 2018. doi: 10.1115/OMAE2018-78661.
- [12] Lu, Y., et al., *A new type connection with optimum stiffness configuration for very large floating platforms*. Proceedings of the Institution of Mechanical Engineers, Part M: Journal of Engineering for the Maritime Environment, 2021. **236**(3): p. 764-778
- [13]. Young-Jun You, Y.-J.J., Min-Su Park, Du-Ho Lee, *Study on Connecting Method of Box Pontoons*. International Journal of Civil and Environmental Engineering, 2014.
- [14] D. Jiang, K. H. Tan, C. M. Wang, and J. Dai, “Research and development in connector systems for Very Large Floating Structures,” *Ocean Engineering*, vol. 232, p. 109150, Jul. 2021, doi: 10.1016/j.oceaneng.2021.109150.
- [15] Z. M. Mohamedmeki, F. J. Esmail, and E. A. Ajeel, “Fatigue life analysis of laminated elastomeric bearing pad,” *Mater Today Proc*, vol. 42, pp. 2361–2368, 2021, doi: 10.1016/j.matpr.2020.12.328.
- [16] A. Erkal, S. S. Tezcan, and D. F. Laefer, “Assessment and Code Considerations for the Combined Effect of Seismic Base Isolation and Viscoelastic Dampers,” *ISRN Civil Engineering*, vol. 2011, pp. 1–10, Oct. 2011, doi: 10.5402/2011/861451.
- [17] Y. Huang, Y. He, Y. Liu, M. Qiu, M. Li, and Z. Luo, “Application and analysis of elastomeric supporting style for topside modules of a spread mooring FPSO,” *Ocean Engineering*, vol. 261, p. 112183, Oct. 2022, doi: 10.1016/j.oceaneng.2022.112183.
- [18] K. Narynbek Ulu, B. Huneau, P.-Y. le Gac, and E. Verron, “Fatigue resistance of natural rubber in seawater with comparison to air,” *Int J Fatigue*, vol. 88, pp. 247–256, Jul. 2016, doi: 10.1016/j.ijfatigue.2016.03.033.
- [19] K. Narynbek Ulu, B. Huneau, P.-Y. le Gac, and E. Verron, “Fatigue resistance of natural rubber in seawater with comparison to air,” *Int J Fatigue*, vol. 88, pp. 247–256, Jul. 2016, doi: 10.1016/j.ijfatigue.2016.03.033.
- [20] National Cooperative Highway Research Program (NCHRP)  
[https://www.trb.org/publications/nchrp/nchrp\\_rpt\\_596.pdf](https://www.trb.org/publications/nchrp/nchrp_rpt_596.pdf)
- [21] Shabana, A. (2020). *Dynamics of Multibody Systems*. Cambridge: Cambridge University Press. doi:10.1017/9781108757553

- [22] Babarit A and Delhommeau G, “Theoretical and numerical aspects of the open source BEM solver NEMOH,” in *11th European Wave and Tidal Energy Conference (EWTEC2015)*, 2015.
- [23] <https://personalpages.manchester.ac.uk/staff/david.d.apsley/lectures/hydraulics3/slides/WaveStatistics.pdf>
- [24] M. Flikkema and O. Waals, “Space@Sea the Floating Solution,” *Front Mar Sci*, vol. 6, Sep. 2019, doi: 10.3389/fmars.2019.00553.
- [25] AASHTO M 251, 2006 Edition, 2006 - Standard Specification for Plain and Laminated Elastomeric Bridge Bearings

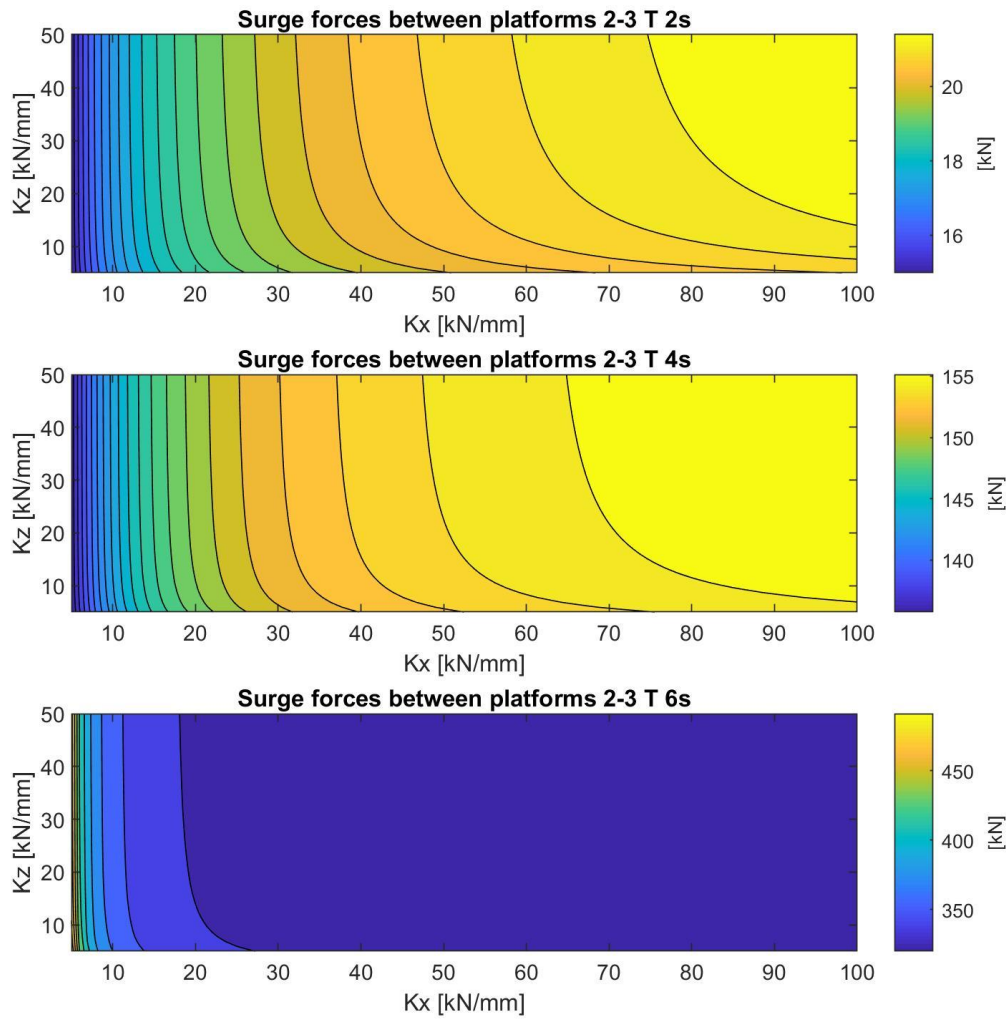
# Appendix



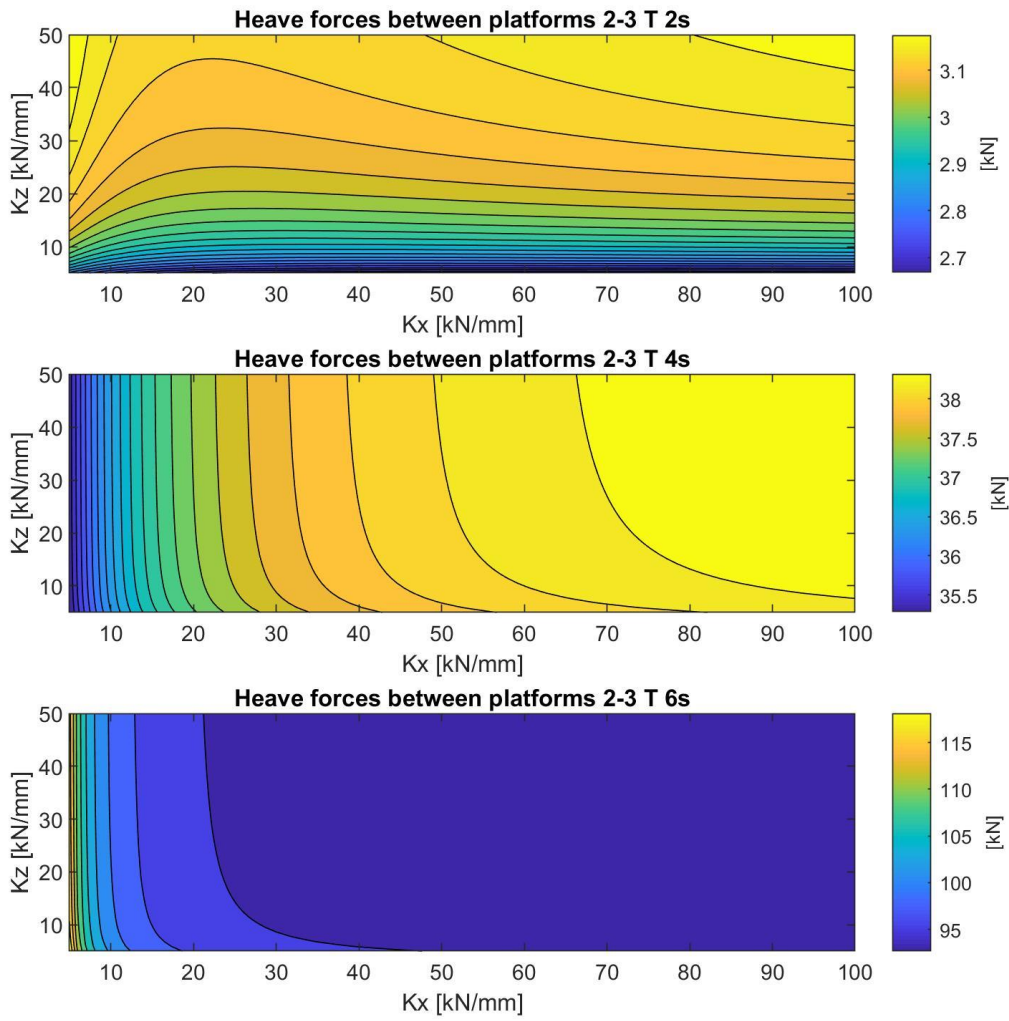
*RAO – max deformations between platforms 2-3 for variable  $K_x$  and  $K_z = 0.5 K_x$*



*RAO – max forces between platforms 2-3 for variable  $K_x$  and  $K_z = 0.5 K_x$*



*Maps – max. surge forces between platforms 2-3 for  $T = 2-4-6$  s*



*Maps – max. surge forces between platforms 2-3 for  $T = 2-4-6$  s*